the plant journal

SEB SOCIETY FOR EXPERIMENTAL BIOLOGY

The Plant Journal (2022) **111,** 1780–1800 doi: 10.1111/tpj.15924

Lysine acetylation regulates moonlighting activity of the E2 subunit of the chloroplast pyruvate dehydrogenase complex in *Chlamydomonas*

Daniel Neusius[1], Laura Kleinknecht[1], Jing Tsong Teh[1], Matthias Ostermeier[1], Simon Kelterborn[2,†], Jürgen Eirich[3], Peter Hegemann[2], Iris Finkemeier[3], Alexandra-Viola Bohne[1] and Jörg Nickelsen[1,*]

[1]*Molecular Plant Sciences, Faculty of Biology, LMU Munich, Großhaderner Str. 2-4, 82152 Planegg-, Martinsried, Germany,*
[2]*Experimental Biophysics, Institute of Biology, Humboldt University of Berlin, Invalidenstr. 42, 10115, Berlin, Germany,*
[3]*Institute of Plant Biology and Biotechnology, University of Muenster, Schlossplatz 7, 48149, Münster, Germany*

Received 26 April 2022; revised 8 July 2022; accepted 18 July 2022; published online 28 July 2022.
*For correspondence (e-mail: joerg.nickelsen@lrz.uni-muenchen.de).
[†]Present address: Charité – Universitätsmedizin Berlin, Institut für Vegetative Physiologie, Charitéplatz 1, 10117, Berlin, Germany

SUMMARY

The dihydrolipoamide acetyltransferase subunit DLA2 of the chloroplast pyruvate dehydrogenase complex (cpPDC) in the green alga *Chlamydomonas reinhardtii* has previously been shown to possess moonlighting activity in chloroplast gene expression. Under mixotrophic growth conditions, DLA2 forms part of a ribonucleoprotein particle (RNP) with the *psbA* mRNA that encodes the D1 protein of the photosystem II (PSII) reaction center. Here, we report on the characterization of the molecular switch that regulates shuttling of DLA2 between its functions in carbon metabolism and D1 synthesis. Determination of RNA-binding affinities by microscale thermophoresis demonstrated that the E3-binding domain (E3BD) of DLA2 mediates *psbA*-specific RNA recognition. Analyses of cpPDC formation and activity, as well as RNP complex formation, showed that acetylation of a single lysine residue (K197) in E3BD induces the release of DLA2 from the cpPDC, and its functional shift towards RNA binding. Moreover, Förster resonance energy transfer microscopy revealed that *psbA* mRNA/DLA2 complexes localize around the chloroplast's pyrenoid. Pulse labeling and D1 re-accumulation after induced PSII degradation strongly suggest that DLA2 is important for D1 synthesis during *de novo* PSII biogenesis.

Keywords: lysine acetylation, DLA2, RNA binding, chloroplast pyruvate dehydrogenase complex, *psbA*, *Chlamydomonas*, dihydrolipoamide acetyltransferase, moonlighting, microscale thermophoresis, Förster resonance energy transfer.

INTRODUCTION

Cellular metabolism and gene expression are tightly interlinked. This becomes particularly important during acclimation processes required to cope with changes in the environment and/or the metabolic status of a cell. In mammals and bacteria, several lines of evidence indicate that gene expression is modulated by intermediates of carbon metabolism (Barańska et al., 2013; Wellen and Thompson, 2012). For instance, some glycolytic enzymes in the cytoplasm also act as regulators of transcription, mRNA stabilization, and translation under specific metabolic conditions, a feature known as 'moonlighting activity' (Jeffery, 2003). Since these enzymes often catalyze rate-limiting steps in metabolic pathways, they are ideally suited for mediating bilateral communication between gene expression and C metabolism under fluctuating environmental/metabolic conditions (Kim and Dang, 2005).

However, our knowledge of the relevant regulatory principles in chloroplasts – which serve as the major hub for C metabolism in photosynthetic eukaryotes – is sparse (Bohne and Nickelsen, 2017; Kleine et al., 2021). The few examples of moonlighting factors so far described in plastid gene expression include a sulfite reductase involved in the compaction of chloroplast nucleoids (Sekine et al., 2002). A second case is represented by the ribulose bisphosphate carboxylase/oxygenase (Rubisco) from the green alga *Chlamydomonas reinhardtii* (*Chlamydomonas*), which catalyzes CO_2 fixation in the first step of the Calvin cycle. Under oxidizing conditions, its large subunit (RbcL) acquires an RNA-binding activity that mediates feedback control of the translation of *rbcL* mRNA and/or the

formation of chloroplast stress granules, which sequester oxidized RNAs (Cohen et al., 2006; Zhan et al., 2015). Moreover, a plastid UMP kinase (PUMPKIN) has recently been shown to bind to intron regions of chloroplast transcripts, thus linking RNA and pyrimidine metabolism, in *Arabidopsis thaliana* (Schmid et al., 2019).

A direct molecular connection between chloroplast gene expression and fatty acid metabolism has been discovered in *Chlamydomonas* chloroplasts with the unexpected finding that the dihydrolipoyl acetyltransferase subunit DLA2 of the chloroplast pyruvate dehydrogenase complex (cpPDC) possesses an intrinsic RNA-binding activity (Bohne et al., 2013b). The cpPDC complex is a megadalton-sized complex consisting of multiple copies of three enzymatic components, i.e., the pyruvate dehydrogenase subunits E1α and E1β (known as PDC2 and PDH2 in *Chlamydomonas*), dihydrolipoamide acetyltransferase E2 (DLA2), and dihydrolipoyl dehydrogenase E3 (DLD2; Mooney et al., 1999; for an overview on PDC structure see Patel et al., 2014; Zhou et al., 2001). This giant enzyme complex catalyzes the oxidative decarboxylation of pyruvate to acetyl-CoA, the initial reaction in chloroplast fatty acid synthesis. However, under favorable mixotrophic growth conditions, i.e., in the presence of light as well as acetate – but not under photoautotrophic or heterotrophic conditions – a thylakoid membrane-associated ribonucleoprotein particle (RNP) containing DLA2 was detected (Bohne et al., 2013b; Ossenbühl et al., 2002). This RNP is specifically associated with the 5′ untranslated region (UTR) of the *psbA* mRNA that encodes the D1 protein of the photosystem II (PSII) reaction center (Bohne et al., 2013b; Ossenbühl et al., 2002).

Moreover, it was shown that *psbA* mRNA can inhibit cpPDC activity in chloroplast extracts, further supporting the idea of a reciprocal functional relationship between gene expression and fatty acid synthesis via a moonlighting activity of DLA2 (Bohne et al., 2013b). Moreover, DLA2 appears to be involved in an acetate-dependent relocalization of *psbA* mRNA to a translation (T)-zone in the vicinity of the chloroplast's pyrenoid (Bohne et al., 2013b; Uniacke and Zerges, 2007). Thus, it was hypothesized that elevated levels of chloroplast acetyl-CoA signal saturation levels of carbon input for fatty acid synthesis, leading to product inhibition of the cpPDC and its partial disassembly. The released DLA2 would then be available for RNP formation with *psbA* mRNA, supporting its transport to T-zones for PSII biogenesis. In this way, DLA2 could mediate the coordination of lipid and protein synthesis during the *de novo* generation of photosynthetic membranes in a light- and acetate-dependent manner (Bohne and Nickelsen, 2017; Bohne et al., 2013b).

The data presented here provide initial insights into the mechanism underlying the shuttling of DLA2 between the cpPDC and an RNP. We show that this process is regulated by reversible acetylation of a lysine in the E3-binding domain (E3BD) of DLA2, which is accompanied by a decrease in cpPDC stability and a concomitant increase in DLA2's association with mRNA on thylakoid membranes. We also show that the resulting DLA2-containing RNP plays a role in the regulation of D1 synthesis for *de novo* biogenesis of PSII.

RESULTS

Only the DLA2 subunit of the cpPDC forms part of an RNP

The DLA2 protein in *Chlamydomonas* was previously shown to be an active subunit of the cpPDC complex (Bohne et al., 2013b). However, when grown under mixotrophic conditions, i.e., in the presence of light and acetate, DLA2 was identified as an integral component of an RNP that contains *psbA* mRNA (Bohne et al., 2013b; Ossenbühl et al., 2002).

To test whether other subunits of the cpPDC form part of an RNP, we analyzed native PDC2 (E1α)-, PDH2 (E1β)-, and DLD2 (E3)-containing complexes by size-exclusion chromatography (SEC) as previously described (Bohne et al., 2013b). In brief, stromal as well as detergent-solubilized thylakoid membrane proteins were prepared from wild-type (WT) cells cultured under mixotrophic conditions, treated with RNase or not, and then subjected to SEC. The elution profiles of cpPDC's subunits were determined by immunodetection using respective antibodies (Figure 1). As reported earlier, DLA2 is found in a membrane-associated, high-molecular-weight (HMW) complex in the megadalton range, which includes an RNA moiety – as indicated by a decrease in the size of the particle upon treatment of solubilized thylakoid membranes with RNases (Figure 1a; Bohne et al., 2013b). In contrast to DLA2, the other membrane-associated cpPDC subunits form smaller complexes in the approximately 400 to 1000 kDa range (fractions 7–9, Figure 1a). These complexes are insensitive to RNase digestion, indicating that they do not represent RNPs (Figure 1a), and they are smaller than expected for a fully assembled cpPDC. This might be a general feature of membrane-associated cpPDC units and/or might be attributable to the known instability of the cpPDC during the solubilization of thylakoid membranes (Bohne et al., 2013b; Camp and Randall, 1985; Treede and Heise, 1986). However, the stromal cpPDC complexes were detected over a wider size range, extending to approximately 20 MDa in the case of PDH2 and DLD2 subunits (Figure 1b).

In agreement with previous results (Bohne et al., 2013b), no RNase-dependent size shift of DLA2 material was observed when soluble stromal fractions were analyzed (Figure 1b). Similarly, no size shift was observed in the other subunits of cpPDC upon treatment of the soluble fractions with RNase (Figure 1b). These data substantiate

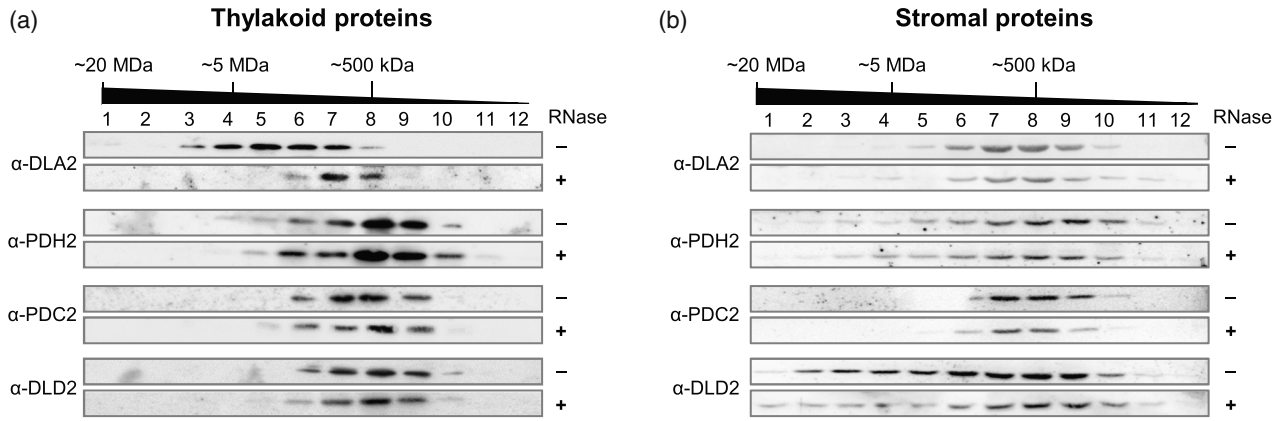

Figure 1. DLA2 is the only cpPDC subunit being a component of a membrane-associated RNP complex. For SEC analysis of cpPDC subunits, solubilized thylakoid (a) or stromal (b) proteins obtained from the cell-wall-deficient WT strain *CC-406* grown under mixotrophic conditions were either treated with (+) RNase or not (–) before loading onto the column. Fractions 1–12 were collected and 10% of each fraction was subjected to electrophoresis on an SDS gel. cpPDC subunits were detected by immunoblotting using the antibodies indicated on the left.

the idea that DLA2 is the only RNA-binding cpPDC subunit that plays a role in the regulation of chloroplast gene expression by shuttling from the metabolic enzyme complex to the membrane-associated RNP containing *psbA* mRNA.

RNA binding by DLA2 is mediated by two distinct protein domains

Like PDC E2 subunits in other species, DLA2 from *Chlamydomonas* has a multidomain structure, comprising an N-terminal lipoyl-binding domain, an E3BD, and a large C-terminal 2-oxo-acid dehydrogenase catalytic domain (Bohne et al., 2013b; Patel et al., 2014). Bioinformatic analysis performed by Bohne et al. (2013b) had previously shown that most of the amino acids predicted to have a high probability for RNA binding are located within the E3BD (Figure S1). Since this domain provides the interaction surface for the DLD2 (E3) subunit of the cpPDC, we performed competitive *in vitro* RNA binding experiments using recombinant DLA2 and DLD2, as well as a radiolabeled *in vitro* transcribed *psbA* 5′ UTR RNA probe (Figure 2). An adenosine-rich region within the 5′ UTR of the *psbA* mRNA is essential for its recognition by native DLA2 from thylakoid membrane fractions (Ossenbühl et al., 2002). Accordingly, the RNA probe used here for the analysis of recombinant proteins covered 96 nucleotides of the *psbA* mRNA including the A-stretch (positions −91 to +5 relative to the AUG start codon).

As reported by Ossenbühl et al. (2002) for native DLA2 from thylakoid membrane protein extracts, also recombinant DLA2 radiolabeled via the crosslinked 5′ UTR RNA probe migrated with an apparent molecular weight of 63 kDa upon SDS-PAGE (Figure 2a, left panel, lane 3). In contrast, no evidence for RNA binding was detected when the recombinant DLD2 was used, confirming the *in vivo* observation that DLD2 is not found in an RNP (Figure 1; Figure 2a, left panel, lane 2). Nevertheless, when DLD2 was added in increasing amounts (up to 10-fold molar excess) to the DLA2 RNA binding reaction, the signal at 63 kDa was titrated out, indicating competition between DLD2 and *psbA* mRNA for DLA2 binding (Figure 2a, lanes 4–6). A comparable titrating effect was not observed when DLD2 was replaced by recombinant glutathione *S*-transferase (GST), which served as control for the specificity of the interaction (Figure 2a, right panel). This strongly supports the idea that the E3BD of DLA2 not only serves as the binding site for DLD2, but is also required for the interaction with *psbA* mRNA.

To further substantiate this conclusion, microscale thermophoresis (MST) experiments were performed to analyze RNA–ligand interactions (Moon et al., 2018). The synthetic Cy5-labeled *psbA* RNA probe employed for MST experiments consisted of the A-rich stretch including 41 nucleotides of the *psbA* mRNA between positions −36 and +5 relative to the AUG start codon (Figure 2b). As summarized in Figure 2b, the affinity of various mutated versions of DLA2 for the *psbA* 5′ UTR RNA probe was quantified (Figures S2–S4). Determination of the affinity of WT DLA2 for this RNA sequence relative to that of an unrelated negative control protein, i.e., PratA (Stengel et al., 2012), showed a clear concentration-dependent fluorescence shift of MST traces for the DLA2 protein indicative of binding to the RNA probe (Figure S3). Analysis of this shift revealed a K_D value of 106 nM (Figure 2b, DLA2), slightly higher than that previously determined (51 nM) using a radioactive filter-binding assay (Bohne et al., 2013b). This deviation is likely due to the different experimental set-ups.

Mutated versions of recombinant DLA2 were then tested *in vitro* to identify the protein regions involved in RNA binding (Figure 2b; Figures S2 and S4). When DLA2's

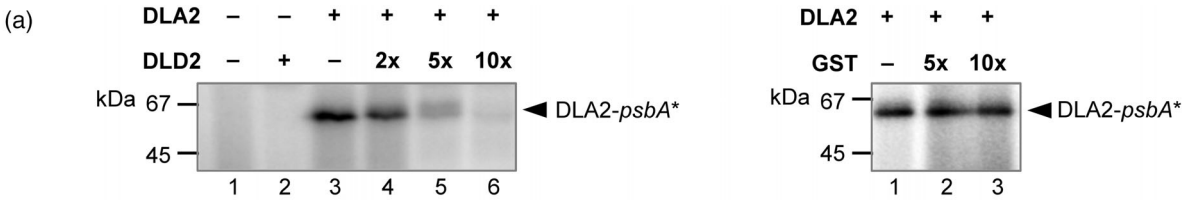

(b) -36 +1 +5
Cy5 **UUUACGGAGAAAUUAAAACUUUAAAAAAAUUAACAU*AUG*AC** Native *psbA* 5′-UTR probe

Protein	Name	K_D [nM]	Relative Affinity [%]
LD – E3BD – Catalytic domain	DLA2	106 ± 24	100
E3BD – Catalytic domain	ΔLip	107 ± 20	99.1
LD – ------ – Catalytic domain	ΔE3B	241 ± 21*	44.0
LD – E3BD – Catalytic domain	ΔCat 462	427 ± 55*	24.8
LD – E3BD – Catalytic domain	ΔCat 450	466 ± 65*	22.7
LD – E3BD	ΔCat 394	558 ± 77*	19.0
LD – E3BD	ΔCat 315	607 ± 82*	17.5
LD – E3BD	ΔCat	911 ± 60*	11.6

(c) -36 +1 +5
Cy5 **UUUACGGAGAAAUUAAAACUUUCCCCCCCCCCCCCAU*AUG*AC** C-stretch *psbA* 5′-UTR probe

Protein	Name	K_D [nM]	Relative Affinity [%]
LD – E3BD – Catalytic domain	DLA2	248 ± 54*	42.7
LD – ------ – Catalytic domain	ΔE3B	244 ± 43	43.4
LD – E3BD – Catalytic domain	ΔCat 462	625 ± 75*	16.9

Figure 2. *psbA* mRNA binding by DLA2. (a) Quantification of competition for the *psbA* 5′ UTR RNA between recombinant DLD2 and DLA2. A radiolabeled *psbA* RNA probe was UV-crosslinked to 2 pmol DLA2 in the presence of 2×, 5×, and 10× molar excess of DLD2 (left panel). To exclude binding of the *psbA* RNA probe to DLD2, a reaction using 100 ng of DLD2 instead of DLA2 was included as control. To show that the competing effect is caused specifically by DLD2, GST protein, instead of DLD2, was added in 5× and 10× molar excess as negative control (right panel). (b, c) The binding affinity of different DLA2 mutant proteins for a native (b) as well as for a mutated ((c), C-stretch) Cy5-labeled 5′ UTR *psbA* probe was measured using MST. Sequences of the native *psbA* 5′ UTR probe and a mutated probe with a C-stretch (red letters) replacing the native A-stretch (green letters) are shown on top of the panels. Positions relative to the start codon (italics) are marked above the sequences. A schematic representation showing the domain structure of the analyzed recombinant proteins is displayed in the left column. The dissociation constants (K_D) displayed are the means (±standard deviation) of three independent experiments. For ease of comparison, binding affinities are also expressed relative to the affinity of the WT protein for the native probe (b) or relative to the affinity of the same protein for the native *psbA* probe (c). The amino acid numbers given in protein names refer to the first deleted amino acid in the respective protein. If no amino acid number is indicated the respective domain was deleted completely. An asterisk indicates that the mean binding affinity of the protein for the respective probe differs significantly from the mean binding affinity of the respective protein for the native *psbA* probe, as determined by a two-sample *t*-test ($P < 0.05$). For Coomassie blue-stained SDS-polyacrylamide gels of the recombinant proteins used for MST analysis, see Figure S2. The respective MST curves are shown in Figures S3 and S4.

lipoyl-binding domain was deleted, no difference in RNA-binding affinity relative to the WT protein was detected; hence, this domain is apparently not involved in RNA binding (Figure 2b, ΔLip). However, upon deletion of the E3BD, the RNA-binding affinity was reduced by 56% compared to the WT protein (Figure 2b, ΔE3B). Furthermore, when the catalytic domain was deleted, RNA binding was drastically decreased to 11.6% of the WT level (Figure 2b, ΔCat).

These results indicate that both the E3BD and the catalytic domain contribute to RNA recognition.

To narrow down the RNA-binding region within the large catalytic domain of DLA2, the protein was progressively truncated from the C-terminus. Removal of the last 33 amino acids led to a drastic reduction in RNA binding to 24.8% of the WT level, pointing to a crucial role of the C-terminal end for *psbA* mRNA recognition (Figure 2b; ΔCat 462). When the C-terminal region was further truncated (ΔCat 450, ΔCat 394, ΔCat 315), the affinity for RNA further decreased to 17.5% of the WT level (Figure 2b). This suggests that the catalytic domain, especially its extreme C-terminal segment, is required for the RNA-binding capacity of DLA2.

The existence of two apparently distinct RNA-binding regions in DLA2 raised the question whether both of them recognize the A-stretch of the *psbA* mRNA probe with the same specificity. Therefore, a mutated version of the *psbA* probe was synthesized in which the critical A-stretch was replaced by a C-stretch (Figure 2c). When this RNA probe was subjected to MST analysis, a significant reduction in binding affinity of DLA2 (to 42.7% of that measured for the native probe) was observed, in line with previous results (Figure 2c; Figure S4b; Ossenbühl et al., 2002). A related, C-stretch-dependent reduction was also observed for the residual activity of the C-terminally truncated DLA2 version (Figure 2c; ΔCat 462), indicating that the truncated protein is still able to discriminate between the C-stretch and the native *psbA* probe. However, the DLA2 mutant protein lacking the E3BD was unable to distinguish between the two RNA probes, as indicated by almost identical relative RNA-binding affinities of approximately 43–44% (Figures 2b,c; ΔE3B).

Taken together, binding of the *psbA* mRNA by DLA2 is mediated by two domains. The C-terminal catalytic domain is crucial for overall RNA binding, whereas the E3BD is responsible for *psbA*-specific RNA recognition.

Reversible lysine acetylation of DLA2 does not alter its RNA-binding affinity

Even though MST analysis yielded significant insights into the RNA-binding mode of DLA2, the underlying regulatory mechanism that determines this function remained elusive.

The higher levels of DLA2 detected in RNPs under mixotrophic conditions cannot be attributed to the availability of larger amounts of DLA2, as equal quantities of the protein were observed under photoautotrophic and mixotrophic growth conditions (Bohne et al., 2013b; Füßl et al., 2022). However, the fact that RNA-binding of DLA2 is dependent on acetate pointed to a potential role for post-translational protein acetylation events. In agreement with this idea, acetylome studies in various organisms have reported acetylation of their respective cpPDC E2 subunits (Chen et al., 2018; König et al., 2014; Mo et al., 2015; Smith-Hammond et al., 2014; Yan et al., 2020). Indeed, a recent analysis of the lysine acetylome of *Chlamydomonas* by Füßl et al. (2022) identified eight lysine acetylation sites in DLA2, i.e., at positions K56, K61, K119, K120, K197, K306, K315, and K394 (Figure S1). Of these, only the acetylation of K197 was significantly and strongly increased 4-fold (adjusted *P*-value < 0.02) under mixo- and heterotrophic conditions compared to photoautotrophic growth, which lacked external acetate. Intriguingly, K197 is located within the E3BD, which is important for both cpPDC assembly and *psbA* mRNA binding. This makes K197 a promising candidate for DLA2's functional switch (Figure S1).

To test whether acetylation at K197 indeed affects the intrinsic RNA-binding activity of DLA2, we performed MST experiments with mutant versions of DLA2 containing amino acid substitutions at K197 (Figure S5). As described first by Ren and Gorovsky (2001), substitution of arginine for lysine mimics the positively charged, non-acetylated state, whereas replacement of lysine by glutamine mimics a constitutively uncharged, acetylated state. Accordingly, K197 in DLA2 was replaced by either glutamine (K197Q) or arginine (K197R). Notably, in addition to K197, the E3BD contains two more lysine residues – K193 and K200 – that were not found to be acetylated *in vivo* (Füßl et al., 2022). These two lysines were investigated in parallel to serve as controls. Neither of the K197 substitutions (K197R, K197Q) resulted in significant changes in DLA2's RNA affinity relative to the WT version (Figure S5). The same is true for mutation of K200 (K200R, K200Q). Interestingly, replacement of K193 by glutamine (K193Q) led to a >50% reduction in RNA-binding activity. Taken together, these data indicate that a potential acetylation-dependent regulatory mechanism at K197 does not affect DLA2's RNA-binding activity directly. In contrast, the presence of a positive charge at position 193 appears to be directly required for RNA binding by DLA2, which further supports a role for the E3BD in RNA recognition.

The acetylation status of lysine residues in the E3BD affects photoautotrophic growth and cpPDC activity

In an earlier study, the phenotypic effects of DLA2 deficiency were monitored in *DLA2* RNA interference (RNAi) strains with residual DLA2 levels of 5–10% (Bohne et al., 2013b). To investigate a mutant phenotype in the complete absence of DLA2 and to obtain a knockout mutant for complementation analyses with DLA2 variants, we generated a *dla2* knockout strain. For this purpose, *DLA2* was inactivated in the arginine auxotrophic strain *CC-3403* by CRISPR/Cas9-mediated insertional inactivation (Greiner et al., 2017; for details see the Experimental Procedures section). In this *dla2* knockout strain, a short DNA fragment interrupts the first exon of the *DLA2* gene, which leads to complete loss of the DLA2

protein (Figure S6a,b). Subsequently, the *dla2* knockout strain was complemented by transformation with a plasmid construct coding for the DLA2 protein fused to a C-terminal HA-tag. Characterization of the *dla2* mutant and the complemented strain (*DLA2-HA*) revealed that loss of DLA2 prevents photoautotrophic growth, whereas complementation with the HA-tagged DLA2 version restored growth on minimal medium (Figure S6b,c). For subsequent experiments, a complemented strain was selected, which accumulates DLA2-HA (approximately 120%) to levels comparable to the amount of DLA2 protein in the WT (Figure S6b). On the other hand, mixotrophic growth in the presence of acetate was not affected in the *dla2* mutant, indicating that the lack of DLA2, and the concomitant loss of cpPDC-mediated production of acetyl-CoA, is fully bypassed by alternative enzymatic activities in the presence of external acetate (Table 1).

To analyze the impact of the acetylation status of the lysine residues in the E3BD on DLA2's function *in vivo*, the *dla2* mutant was transformed with various mutated versions of DLA2-HA, each harboring an acetylation-mimicking glutamine substitution at either K193, K197, or K200, or an acetylation-preventing arginine substitution at K197. The *DLA2-HA* strain was used as reference for the subsequent characterization of resulting mutant lines.

Analysis of doubling times of the various strains revealed that the *K193Q-HA* and *K197Q-HA* mutants grew at reduced rates compared to the *DLA2-HA* reference strain under photoautotrophic conditions (Table 1). On the other hand, the *K197R-HA* strain showed slightly increased growth in high-salt minimal (HSM) medium, whereas *K200Q-HA* grew at rates comparable to *DLA2-HA* (Table 1). Under mixotrophic conditions, all strains grew at similar rates, indicating that acetate can complement the growth phenotype observed in the point-mutant strains under photoautotrophic conditions. Together, the results suggest that the acetylation of K193 and K197 promotes photoautotrophic growth, whereas their deacetylation reduces it.

Table 1 Doubling times (h) of the *CC-3403* WT strain, the *dla2* mutant, the complemented *DLA2-HA* strain, and acetylation mutant strains grown under mixotrophic or photoautotrophic conditions

Strain	Mixotroph	Photoautotroph
CC-3403	10.2 ± 0.9	36.1 ± 5.9
dla2	10.0 ± 0.5	—
DLA2-HA	9.5 ± 0.3	38.8 ± 4.9
K197Q-HA	9.9 ± 0.2	45.3 ± 6.3*
K197R-HA	9.8 ± 0.2	34.4 ± 3.6*
K193Q-HA	9.3 ± 0.3	44.2 ± 5.4*
K200Q-HA	9.7 ± 0.3	35.6 ± 4.3

Values are means ± standard deviation from at least three biological replicates. An asterisk indicates a significantly altered doubling time compared to the *DLA2-HA* reference strain as determined by a two-sample *t*-test ($P < 0.05$).

Next, we tested whether cpPDC accumulation is affected by these point mutations. Immunoblot analysis of DLA2 and the other cpPDC subunits revealed a reduction in levels of cpPDC subunits only in the *dla2* knockout strain, with PDC2 and PDH2 being significantly decreased to about 65 and 75% of WT levels, respectively, whereas DLD2 was decreased to approximately 85% (Figure 3a, Figure S7). In contrast, all DLA2 acetylation strains accumulated cpPDC subunits to the levels seen in the *DLA2-HA* reference strain. Unexpectedly, *K197Q-HA* and *K200Q-HA* exhibited increased accumulation of their respective mutant forms of DLA2-HA (Figure 3a, Figure S7). However, this increase did not correlate with their photoautotrophic growth rates, which were reduced in *K197Q-HA* and unaffected in *K200Q-HA* (Table 1). Therefore, we analyzed whether cpPDC's enzymatic activity is altered by the point mutations at positions K193, K197, and K200. In agreement with their reduced growth rates under photoautotrophic conditions, in the *K193Q-HA* and *K197Q-HA* strains, cpPDC activity was reduced by about 30% and 50% (Figure 3b). Furthermore, in *K197R-HA*, cpPDC activity was elevated to 140%, whereas *K200Q-HA* had a cpPDC activity similar to that of the *DLA2-HA* reference strain (Figure 3b). Again – and in contrast to cpPDC accumulation – a clear correlation was observed between effects on growth and cpPDC enzymatic activity. These data strongly suggest that simulated acetylation at either K193 or K197 leads to reduced cpPDC activity, whereas deacetylation at K197 results in increased cpPDC activity *in vivo*. Hence, the growth phenotypes of the various DLA2 acetylation strains in the absence of acetate can be attributed to altered cpPDC activity (Table 1).

Acetylation at K197 within the E3BD of DLA2 leads to the disassembly of cpPDC

To elucidate how acetylation might affect the activity of the cpPDC, we analyzed the status of the complex in all DLA2 acetylation strains. The tagged DLA2 protein was immunoprecipitated from soluble lysates using a bead-coupled HA antibody, and the amounts of co-precipitated cpPDC subunits were determined by quantification of immunoblot signals (Figure 4). Interestingly, in the *K197Q-HA* strain under mixotrophic conditions, far fewer cpPDC subunits co-precipitated than in the *DLA2-HA* reference strain (Figure 4a, left panel). The amount of DLD2 was decreased to 60%, and amounts of co-precipitated PDH2 and PDC2 were reduced even more, i.e., to 40% and 20% of the control level, respectively. However, upon constitutive deacetylation of DLA2 in the *K197R-HA* strain, the levels of co-precipitated cpPDC subunits were significantly elevated (Figure 4a, left panel). The same pattern was observed under photoautotrophic growth conditions, with elevated levels of cpPDC subunits being co-precipitated in *K197R-HA* and decreased amounts in *K197Q-HA* (Figure 4a, right panel). These data correlate with the measured cpPDC

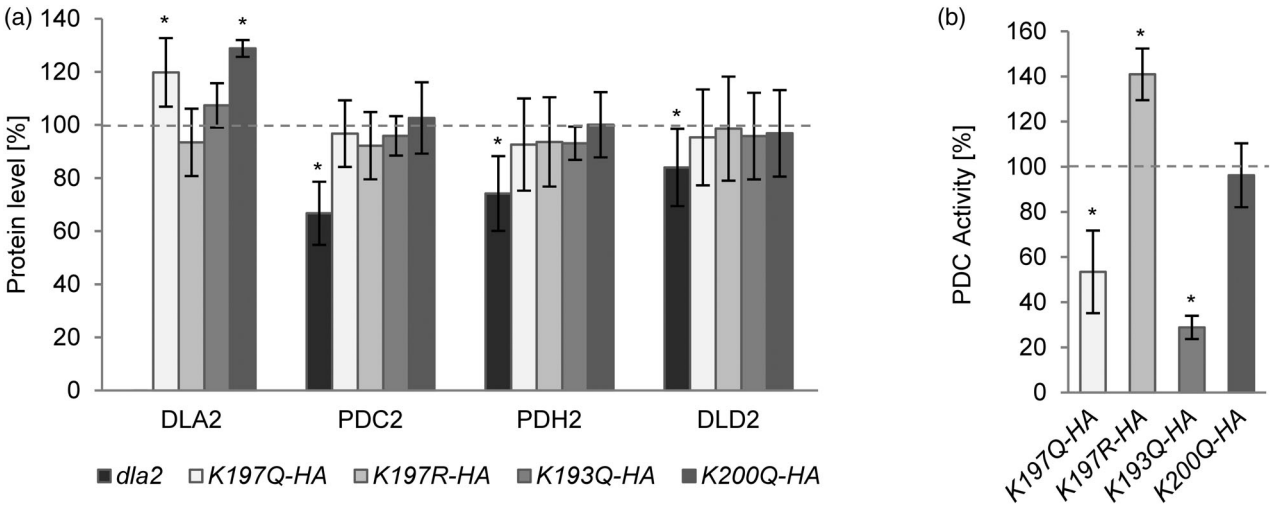

Figure 3. Accumulation of cpPDC subunits and cpPDC activity in DLA2 mutant strains. (a) Loss of DLA2 leads to reduced accumulation of the other cpPDC subunits in various mutant strains. Total cell lysates (15 μg) from each strain were fractionated by SDS-PAGE and subjected to immunoblotting. Protein signals of at least five independent experiments were quantified. The signal in the *DLA2-HA* strain was set to 100%, and the means and standard deviations of the *dla2* mutant and the two acetylation mutants were calculated and are shown on the right. Asterisks indicate that the mean protein accumulation is significantly different from that of the same protein in the *DLA2-HA* strain, as determined by a one-sample *t*-test ($P < 0.05$). Examples of the respective blots can be found in Figure S7. (b) The acetylation state of lysine residues within the E3BD influences cpPDC activity. cpPDC activity tests were performed as described in the Experimental Procedures. The cpPDC activity measured in the *DLA2-HA* strain was set to 100%. Mean values and standard deviations from at least three independent experiments are shown. Asterisks indicate that the mean cpPDC activity of the mutated strain is significantly different from that of the *DLA2-HA* strain (one-sample *t*-test; $P < 0.05$).

activities in both strains (Figure 3b). Thus, simulated acetylation and the concomitant loss of the positive charge at K197 results in a severe decrease in cpPDC stability and leads to reduced metabolic activity. On the other hand, preservation of the positive charge at this position in *K197R-HA* enhances both the stability and catalytic activity of cpPDC (Figures 3b and 4a).

As a control, the *K193Q-HA* and *K200Q-HA* strains, which mimic non-native acetylation events within E3BD, were also analyzed (Figure 4b). Whereas *K200Q-HA* behaved like the *DLA2-HA* reference strain, simulated acetylation at K193 interestingly led to an even stronger reduction in the levels of co-precipitated cpPDC subunits (only 5% of PDC2 and approximately 20% each of PDH2 and DLD2) compared to simulated acetylation at K197 (Figure 4b). This indicates that K193 is a crucial determinant for cpPDC formation in general.

Taken together, these findings strongly suggest that the differential acetylation status of K197 regulates the stability of cpPDC, and therefore its metabolic activity *in vivo*. This in turn contributes to the observed growth phenotypes of the analyzed strains (Table 1).

Acetylation-dependent disassembly of the cpPDC leads to enhanced formation of the native RNP

The data presented so far strongly suggest that acetylation at K197 leads to the disassembly of the cpPDC. In other words, the degree of acetylation determines the amount of free DLA2 that is available for RNP formation with the *psbA* mRNA. Since we have previously shown that this RNP is attached to thylakoid membranes (Bohne et al., 2013b), acetylation at K197 should result in elevated membrane association of DLA2. To test this, we fractionated cell lysates of the *DLA2-HA* strain grown under mixo- and photoautotrophic growth conditions into soluble and membrane fractions, and determined their respective contents of DLA2. While no growth-dependent differences in DLA2 levels could be observed in the soluble fractions (Figure S8a), the amount of DLA2 present in membrane fractions increased to almost 150% under mixotrophic relative to photoautotrophic growth conditions (Figure 5a). This indeed suggests that the increased acetylation of K197 under mixotrophic growth conditions observed by Füßl et al. (2022) might lead to an increase in membrane-associated DLA2. Importantly, the simulation of constitutive acetylation of K197 in the *K197Q-HA* strain enhanced the amounts of DLA2 associated with the membrane under both growth conditions (Figure 5b). On the other hand, a decrease in membrane association of DLA2 under both growth conditions was found in *K197R-HA*, which mimics complete deacetylation of K197 (Figure 5b). Again, no differences in DLA2 accumulation were observed for soluble fractions of these acetylation mutant strains (Figure S8b). Thus, association of DLA2 with the membrane clearly correlates with its acetylation status – further supporting the idea that post-translational modification of K197 plays a crucial role in the regulation of cpPDC activity.

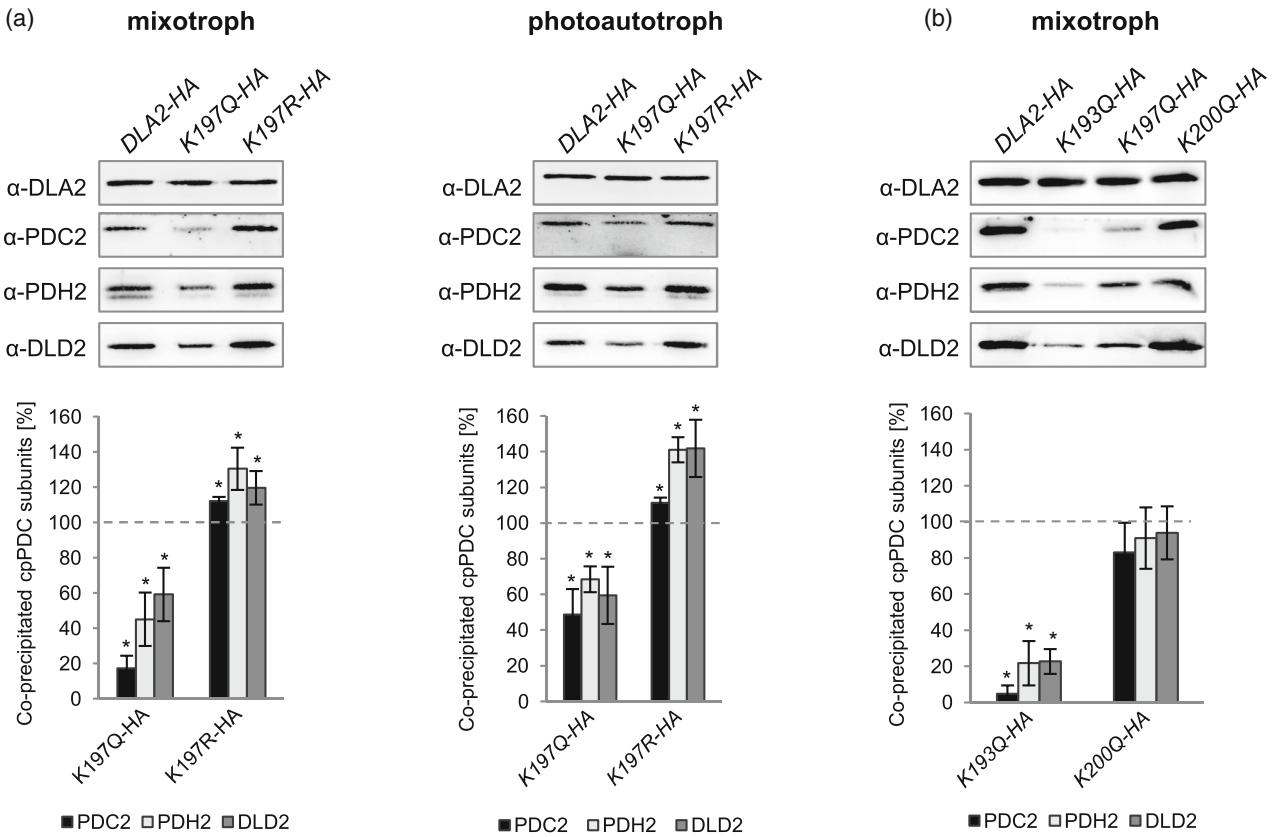

Figure 4. The acetylation state of lysine residues within the E3BD influences the stability of the cpPDC complex. Co-immunoprecipitation of cpPDC subunits using soluble extracts of various *DLA2-HA* acetylation strains by bead-coupled HA antibodies. The precipitates were fractionated by SDS-PAGE and levels of cpPDC subunits were determined by Western blot analysis. The protein signals from three independent experiments were quantified and the corresponding signal in the *DLA2-HA* strain was set to 100%. Mean and standard deviation of the different protein signals in the acetylation mutants was calculated and depicted in the bar diagram. (a) Analysis of K197 acetylation mutants grown under mixotrophic (left panel) or photoautotrophic conditions (right panel). (b) Analysis of K193 and K200 acetylation mutants grown under mixotrophic conditions. For ease of comparison, the Western blot data for *K197Q-HA* are shown here as well. For quantification of *K197Q-HA*, see (a). An asterisk indicates that the mean co-precipitation of the protein in this strain is significantly different from that of the respective protein in the *DLA2-HA* strain, as determined by a one-sample *t*-test ($P < 0.05$).

To determine whether the increase in membrane association of DLA2 upon acetylation of K197 is paralleled by an enhancement of RNP formation, we performed SEC of solubilized membranes obtained from the various strains grown under mixotrophic and photoautotrophic conditions (Figure 6). In the *DLA2-HA* reference strain, a moderate RNase-induced shift of the DLA2 material was detected under mixotrophic conditions – as indicated by stronger signals in HMW fractions 3–6 in the absence of RNase treatment and a relatively strong signal in lower-molecular-weight (LMW) fractions 7–10 after RNase treatment (Figure 6, left panel). Under photoautotrophic growth conditions, no size shift could be detected for *DLA2-HA* (Figure 6, right panel). Strikingly, a marked, RNase-dependent shift from HMW to LMW fractions pointed to a higher level of the RNP in *K197Q-HA* under mixotrophic growth conditions (Figure 6, left panel). Even under photoautotrophic growth conditions, a clear though less pronounced shift of DLA2 material was monitored in the *K197Q-HA* strain, which mimics constitutive acetylation of DLA2 (Figure 6, right panel). This is compatible with the increase in the membrane-associated fraction of DLA2 observed in *K197Q-HA* (compare Figure 5b). In contrast, *K197R-HA* contained no RNase-sensitive DLA2 complex, implying that little or no RNP is formed under either of the growth conditions tested (Figure 6). Again, this is consistent with a reduction in the amount of DLA2 associated with the membrane in this strain (Figure 5b). Taken together, the data suggest that increased disassembly of the cpPDC upon acetylation at K197 of DLA2 leads to an increase in the formation of a DLA2-containing RNP on thylakoid membranes. However, as the increase of RNP formation is more pronounced under mixotrophic as compared to photoautotrophic conditions it can be assumed that beside acetylation of K197 an additional determinant, like unidentified acetylation sites at DLA2 or other cpPDC subunits, promotes RNP formation in an acetate-dependent manner.

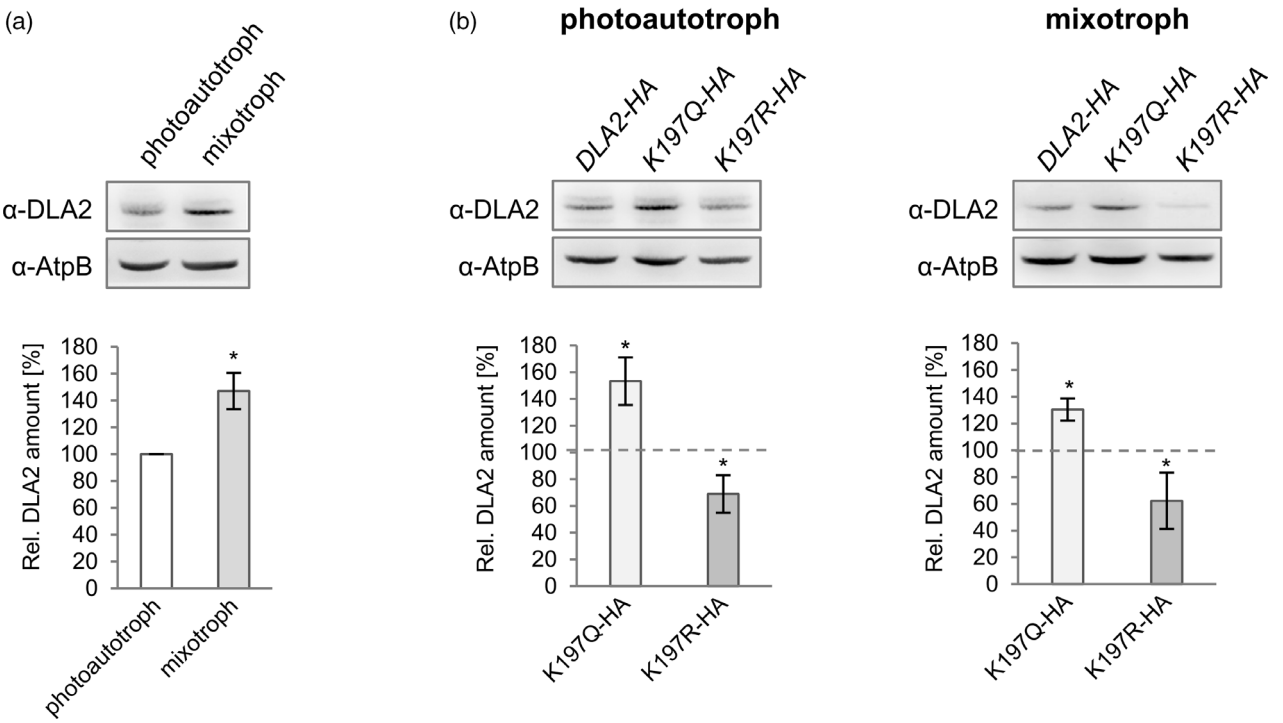

Figure 5. Mimicked acetylation of K197 enhances the membrane association of DLA2. Solubilized membrane proteins (40 μg) were fractionated by SDS-PAGE and subjected to Western blot analysis, and the level of DLA2 accumulation was normalized to the amount of AtpB in the membrane fraction. Blots of the corresponding soluble fractions are shown in Figure S8. (a) Relative levels of membrane-associated DLA2 in the *DLA2-HA* strain under photoautotrophic or mixotrophic conditions. DLA2/AtpB signal intensities obtained for photoautotrophic conditions were set to 100%. Asterisks indicate that the mean DLA2/AtpB ratio is significantly different from that under photoautotrophic conditions. (b) Membrane-associated DLA2 in the *DLA2-HA* strain and K197 acetylation mutants under photoautotrophic and mixotrophic conditions. Membrane-associated DLA2 in the *DLA2-HA* strain was set to 100% and is depicted as a gray dotted line. All means and standard deviations are calculated from at least three independent experiments. Asterisks indicate that the mean DLA2/AtpB ratio is significantly different from that in the *DLA2-HA* strain as determined by a one-sample *t*-test ($P < 0.05$).

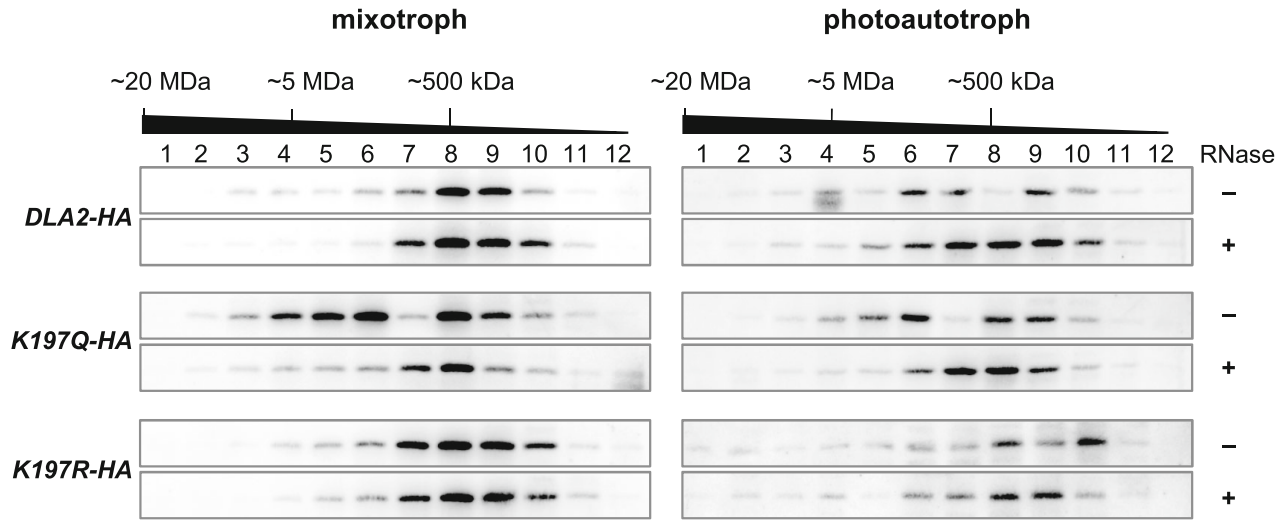

Figure 6. The acetylation state of K197 influences RNP formation. SEC of thylakoid fractions 1–12 from K197 acetylation strains (*K197Q-HA* and *K197R-HA*) and the *DLA2-HA* reference strain grown under mixotrophic and photoautotrophic growth conditions as indicated. Solubilized thylakoids were either treated with (+) RNase or not (–) prior to SEC. Fractions were collected, and 10% of each fraction was loaded on an SDS gel and subjected to electrophoresis. DLA2 complexes were detected by immunoblotting using anti-DLA2. Analyzed strains are indicated to the left of the panels.

Further, it should be noted that the RNP level in the *DLA2-HA* reference strain was lower than that found in the *CC-406* WT strain shown in Figure 1(a). This might be due to the presence of the triple HA-tag at the C-terminus of DLA2 in *DLA2-HA*. Since the progressive deletion of the C-terminal portion of recombinant DLA2 led to a gradual

decrease in RNA-binding affinity during MST experiments (Figure 2b), this region appears to be important for RNP formation. Accordingly, a C-terminally positioned HA-tag might lead a reduction in the stability of the RNP. Such an effect would be particularly noticeable due to the protracted preparation of the thylakoid membranes and their subsequent fractionation by SEC.

To minimize such potential effects of the HA-tag and improve detection of the RNP containing both DLA2 and *psbA* mRNA, we looked for another method that would allow faster processing of the cells. We chose Förster resonance energy transfer (FRET) microscopy for this purpose, as it has previously been shown to be suitable for visualization of RNA–protein interactions in human cells (Huranová et al., 2009; Lorenz, 2009). This method includes an early fixation step, followed by fluorescence *in situ* hybridization (FISH) with ATTO 488 fluorophore-coupled oligonucleotides specific for *psbA* mRNA and immunofluorescence (IF) staining using a DyLight 550 fluorophore-coupled antibody that recognizes the HA-tag. Subsequently, fluorescence microscopy was performed and the chromophore label of the *psbA* mRNA was specifically excited using the appropriate wavelength. If both chromophores are in close proximity (<5 nm apart), the emission energy of the chromophore attached to the *psbA* mRNA excites the chromophore on the DLA2-HA fusion protein. If a fluorescence signal emitted by the second chromophore can be detected, the very close physical proximity of DLA2 and the *psbA* mRNA strongly suggests that they interact directly with each other in the RNP.

When considered individually, no obvious differences in the spatial distribution of the *psbA* mRNA and the DLA2-HA signals were detected between strains or between growth conditions (Figure 7; Figures S9 and S10). The highly abundant *psbA* mRNA was dispersed all over the chloroplast, whereas the DLA2-HA signal was localized in punctate patterns that often appeared to surround the pyrenoid of the chloroplast – a sub-organellar, phase-separated compartment in which Rubisco catalyzes carbon fixation under ambient conditions (He et al., 2020; Wang et al., 2015). As negative controls for the interaction assay, the *dla2* knock-out strain and the chloroplast *FuD7* mutant lacking the *psbA* gene were analyzed in parallel (Bennoun

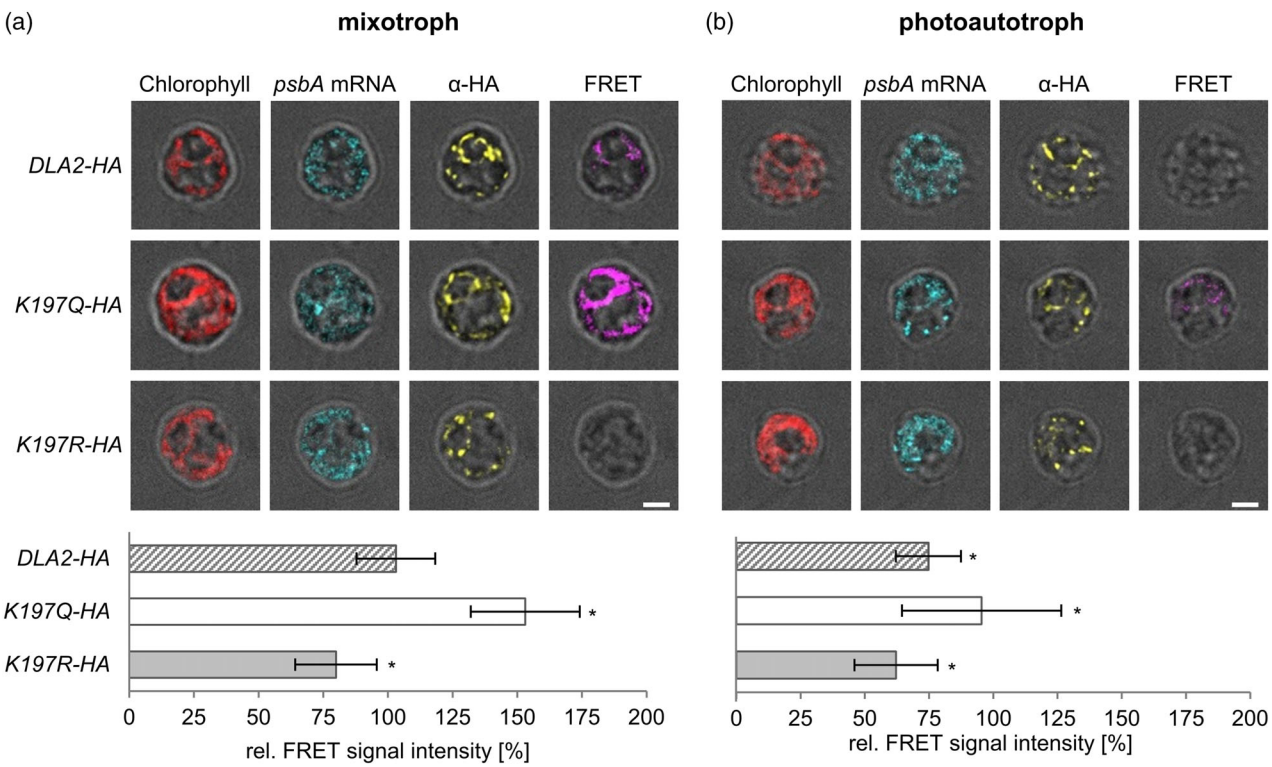

Figure 7. Mimicked acetylation at K197 forces the interaction of DLA2-HA and *psbA* mRNA. Fluorescence micrographs of the *DLA2-HA* strain and the *K197Q-HA* and *K197R-HA* acetylation strains under (a) mixotrophic and (b) photoautotrophic conditions. Chlorophyll autofluorescence (red), fluorescence *in situ* hybridization (FISH) of the *psbA* mRNA (cyan), immunofluorescence (IF) of the DLA2-HA protein (yellow), and Förster resonance energy transfer (FRET) signals visualizing the DLA2–*psbA* interaction (purple) are depicted. Quantification was performed using ImageJ and the ratio of the FRET signal to the DLA2-HA signal was calculated. The mean value obtained for the *DLA2-HA* strain under mixotrophic conditions was set to 100%. Mean values and standard deviations calculated from at least 10 cells are shown. Asterisks indicate that the mean signal ratio for this strain is significantly different from that of the *DLA2-HA* strain under mixotrophic growth conditions, as determined by a two-sample *t*-test ($P < 0.05$). Scale bar = 2 μm.

et al., 1986). Indeed, neither DLA2 nor *psbA* mRNA signals were detected in the respective assays (Figure S11a,b). Moreover, no distinct FRET signal was detected in the *DLA2-HA* line when a FISH probe that bound to the unrelated *psaA* transcript that is not expected to bind to DLA2 was used (Figure S11c).

In contrast to the controls, DLA2/*psbA* FRET signals clearly varied depending on the analyzed strains and the growth conditions employed (Figure 7; Figures S9 and S10). Strikingly, quantification of the FRET signals revealed that the signal intensity in the *K197Q-HA* strain was increased by 50% relative to the *DLA2-HA* reference strain when cells were grown mixotrophically (Figure 7a). On the other hand, the FRET signal intensity in *K197R-HA* was reduced to approximately 80%, suggesting that the RNP was less abundant. Moreover, this correlated directly with the RNP levels detected upon SEC (Figure 6, left panel). Under photoautotrophic growth conditions, the FRET signal intensity in *DLA2-HA* was reduced to approximately 70% compared to that obtained under mixotrophic conditions in the same strain (Figure 7b). This reflects the lack of substantial RNP formation in the absence of acetate (Figure 7b; Figure 6, right panel). By contrast, simulated constitutive acetylation at K197 in *K197Q-HA* increased the FRET signal even under photoautotrophic conditions to the rate reached in mixotrophically grown *DLA2-HA* cells (Figure 7). Conversely, constitutive deacetylation at K197 in *K197R-HA* diminished the FRET signal to approximately 60% (Figure 7b). This suggests the accumulation of minor amounts of DLA2-containing RNPs in *DLA2-HA* under photoautotrophic growth conditions, which were not detected by the less sensitive SEC (Figure 6, right panel). In summary, the IF-based visualization of DLA2/*psbA* mRNA complexes confirmed that destabilization of the cpPDC upon acetylation at K197 leads to enhanced RNP formation. Hence, the modification of K197 is the key factor that regulates DLA2's moonlighting activity.

Upon analyzing the spatial distribution of FRET signals, it became evident that most of the *psbA* mRNA–DLA2 interactions are localized at or close to the pyrenoid. This becomes even more obvious when one examines 3D reconstructions of the *DLA2-HA* strain (Movie S1). Uniacke and Zerges (2007) postulated that PSII *de novo* biogenesis in *Chlamydomonas* is located at T-zones adjacent to the pyrenoid. These T-zones are characterized by a dense accumulation of plastid ribosomes and transcripts coding for PSII subunits like D1 (Sun et al., 2019). Moreover, we have previously proposed that DLA2 might be responsible for delivering the *psbA* mRNA to these T-zones for efficient *de novo* biogenesis of PSII under favorable conditions (Bohne et al., 2013b). Hence, this hypothesis is now further supported by the location of FRET signals accumulating around the pyrenoid.

DLA2 is involved in the regulation of D1 synthesis for PSII *de novo* biogenesis

To further explore the impact of DLA2 on D1 synthesis, we performed ^{35}S pulse-labeling experiments in the *dla2* mutant, as well as in the K197 acetylation mutants grown under mixotrophic growth conditions. In agreement with previous pulse-labeling experiments performed on *iDLA2* knockdown lines (Bohne et al., 2013b), the *dla2* knockout mutant exhibited a reduced D1 synthesis rate to 60% as compared to the *DLA2-HA* reference strain, while D1 synthesis in *K197Q-HA* and *K197R-HA* was not affected under these conditions (Figure 8a). However, as reported earlier for *DLA2* RNAi strains (Bohne et al., 2013b), the impact of *DLA2* knockout on D1 synthesis was not reflected by D1 accumulation in *dla2* at steady-state level, suggesting either that D1 translation does not limit the PSII level or that compensatory mechanisms exist under constant environmental conditions (Figure 8b). In line with previous data reported by Bohne et al. (2013b) for *iDLA2* knockdown lines, no significant changes in other photosynthesis-related proteins were detected in *dla2* or the acetylation mutant strains (Figure 8b). This is compatible with the maximum quantum efficiency of PSII (F_v/F_m) of about 0.79 measured in the investigated strains (Table 2).

To distinguish whether reduced D1 synthesis rates in the *dla2* knockout mutant affect D1 synthesis for PSII repair or *de novo* PSII biogenesis at T-zones, photoinhibition experiments were performed. Therefore, D1 accumulation was analyzed after a shift from normal (30 $\mu E\ m^{-2}\ sec^{-1}$) to high light (800 $\mu E\ m^{-2}\ sec^{-1}$) intensities (Figure S12, left panel). All analyzed strains maintained the same constant D1 level over the time course of 1.5 h, indicating that repair synthesis for the replacement of photodamaged D1 is intact. To exclude the possibility that the effect on D1 synthesis observed in the pulse-labeling experiments might be due to an alteration in D1 stability, the experiment was repeated in the presence of plastid translation inhibitors (Figure S12, right panel). This led to a substantial decrease in D1 accumulation over a period of 1.5 h, regardless of the genetic background of the strains. This strongly argues that the reduction in D1 synthesis in the *dla2* mutant affects *de novo* PSII biogenesis rather than PSII repair.

To further test this idea, we analyzed *de novo* PSII biogenesis as described by Malnoë et al. (2014). After inducing degradation of PSII by sulfur depletion for 48 h, re-accumulation of D1 in the context of *de novo* PSII synthesis was induced by sulfur addition, and monitored for another 24 h by immunoblot analysis (Figure 9). Quantification and normalization of the D1 signal to the HSP70B signal revealed no differences among the strains during the initial 48-h phase of sulfur depletion. In contrast, during the following 24 h of sulfur repletion, the *dla2* mutant re-accumulated significantly less D1 than the *DLA2-HA* reference strain. In

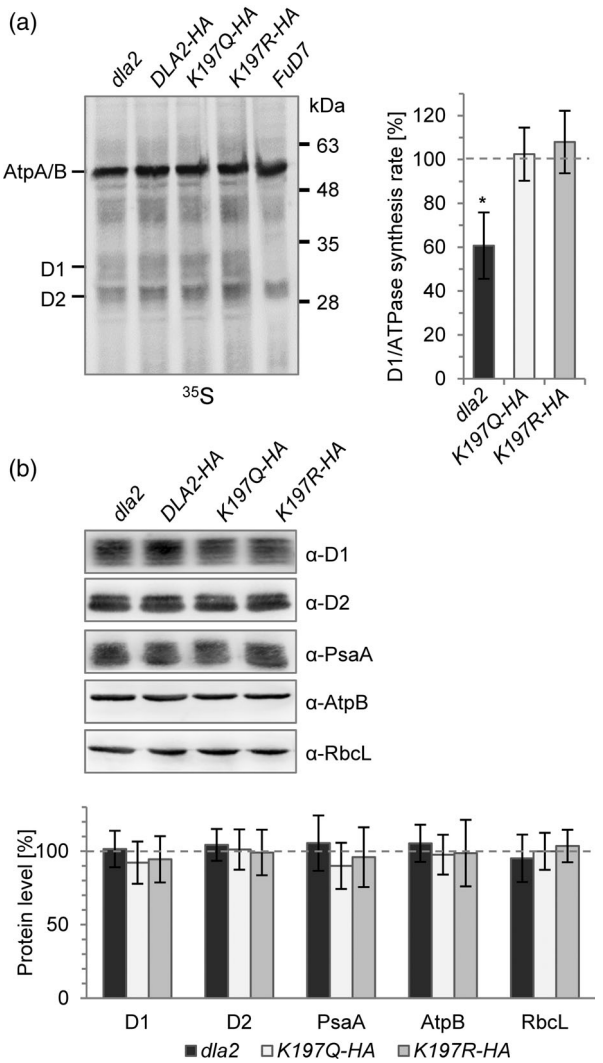

Figure 8. D1 protein accumulation and synthesis in the *dla2* mutant and various complemented strains under mixotrophic growth conditions. (a) ^{35}S pulse-labeling experiment. Whole-cell proteins of indicated strains were pulse-labeled with ^{35}S-sulfate prior to separation by SDS-PAGE. Proteins were then blotted onto a nitrocellulose membrane and analyzed by autoradiography. Quantification of the D1 signal was performed using ImageJ software and its level was normalized to the AtpA/B signal. The values obtained for the *DLA2-HA* strain were set to 100% and means and standard deviations from three independent experiments are shown (right panel). Asterisks indicate a significant difference ($P < 0.05$) to *DLA2-HA* using a one-sample *t*-test. (b) Accumulation of photosynthesis-related proteins. A representative Western blot is shown on top. Quantification of protein signals on Western blots based on at least three independent experiments is shown in the bar diagram at the bottom.

Table 2 F_v/F_m values of the *CC-3403* WT strain, the *dla2* mutant, the complemented *DLA2-HA* strain, and acetylation mutant strains grown under mixotrophic conditions

Strain	F_v/F_m
CC-3403	0.80 ± 0.01
dla2	0.79 ± 0.02
DLA2-HA	0.79 ± 0.01
K197Q-HA	0.80 ± 0.01
K197R-HA	0.79 ± 0.02
K193Q-HA	0.78 ± 0.01
K200Q-HA	0.79 ± 0.02

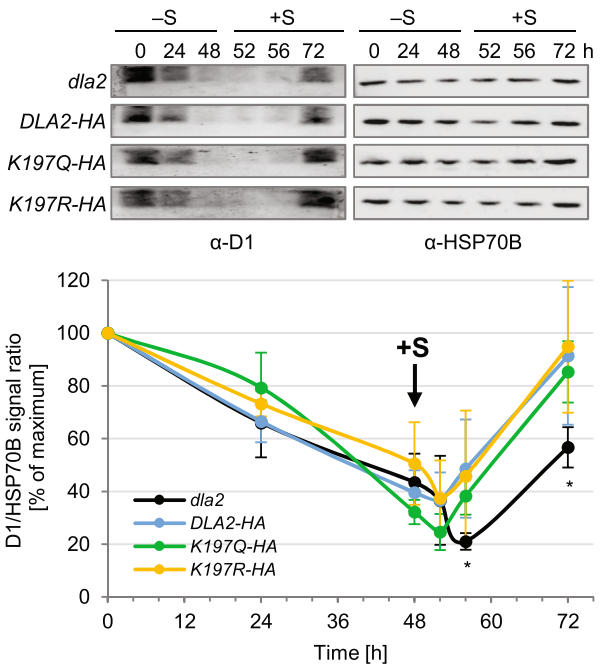

Figure 9. Loss of DLA2 leads to slower accumulation of D1 for *de novo* PSII biogenesis. Liquid cultures of the indicated strains were grown in TAPS to a cell density of about 2 × 10^6 cells ml^{-1} in constant light (30 µE m^{-2} sec^{-1}). Cells were then shifted to medium lacking sulfur (–S). After 48 h under –S conditions, cultures were returned to TAPS medium containing sulfur (+S) for another 24 h. Whole-cell proteins from samples taken at the indicated time points were separated via SDS-PAGE and D1 abundance was measured, using immunoblot analysis and HSP70B as loading control. Quantification of the immunoblot signals was performed using ImageJ software and D1 signals were normalized to the respective HSP70B signals. The values obtained for the time point 0 h were set to 100%.

particular, D1 re-accumulation was delayed between 4 and 8 h of sulfur repletion (Figure 9). This delayed response, together with a slightly lower D1 accumulation rate during the subsequent 16 h, led to a significant reduction in the D1 level of approximately 55% after 24 h of sulfur replenishment. In contrast, D1 accumulation in *DLA2-HA* and the two DLA2 acetylation strains followed the same profile, and was restored to 85–95% after 24 h of sulfur repletion. This suggests that the acetylation status of K197 is not a rate-limiting factor for D1 re-accumulation under these conditions, regardless of its effect on RNP formation. Taken together, these data demonstrate that DLA2 is involved in D1 synthesis for *de novo* PSII biogenesis. Moreover, the delayed D1 accumulation response upon sulfur repletion in the *dla2* mutant suggests that the delivery of *psbA* mRNA to T-zones mediated by DLA2 is a prerequisite for the activation of faster adaptation processes to environmental transitions. However, K197 acetylation alone is not sufficient to mediate the control of D1 synthesis.

DISCUSSION

In recent years, the pyruvate dehydrogenase complex has attracted increasing attention as a moonlighting enzyme involved in the regulation of gene expression, in addition to its enzymatic role in acetyl-CoA production. For instance, subunits of the human mitochondrial PDC have also been localized to the nucleus, where they appear to control gene transcription via interaction with transcription and/or histone acetylation factors (Chen et al., 2018; Richard et al., 2017). The cpPDC subunit DLA2 represents one example of an enzyme in carbon metabolism that moonlights in plastid gene expression in the green alga *Chlamydomonas* (Bohne et al., 2013b). In that context, DLA2 could mediate reciprocal molecular bilateral communication between fatty acid synthesis and protein synthesis, enabling functional coordination of the two pathways for optimal thylakoid membrane biogenesis (Bohne and Nickelsen, 2017). In addition, the acetate-dependent acetylation of K197 recently identified by Füßl et al. (2022) suggests a potential regulatory mechanism for the function of DLA2.

The basis of DLA2-dependent RNA binding

Here, we show that DLA2 is the only cpPDC subunit that forms part of an RNase-sensitive RNP in the megadalton range, as assessed by SEC of solubilized chloroplast membranes (Figure 1a). Moreover, mapping of potential RNA-binding domains within DLA2 revealed that two regions are crucial for efficient RNA recognition (Figure 2). The E3BD region mediates both DLD2 interaction and specific recognition of *psbA* mRNA, suggesting that it represents the critical domain for DLA2's function in gene expression. In agreement with this idea, within the E3BD, K197 is differentially acetylated under mixotrophic and photoautotrophic conditions, and loss of the positive charge at position K193 affects RNA binding (Figure S5; Füßl et al., 2022).

Unexpectedly, deletion of only a few amino acids of the C-terminus results in a severe drop in overall RNA-binding activity, but leaves its RNA-binding specificity intact (Figure 2b). Notably, the C-terminal truncation does not remove residues in the catalytic domain that were bioinformatically predicted to have RNA-binding capacity (Figure S1; Bohne et al., 2013b). Nevertheless, mutation of the C-terminus might induce conformational changes of DLA2 indirectly affecting RNA binding at the E3BD. Overall, the data suggest that the C-terminal region of DLA2 plays a critical role in determining its overall affinity for RNA, whereas the E3BD mediates specific recognition of the *psbA* 5′ UTR.

DLA2's metabolic function is regulated by K197

Analysis of the *dla2* knockout mutant revealed that DLA2 is essential for photoautotrophic growth (Figure S6). This is compatible with data published by Wakao et al. (2021), who recently identified a *Chlamydomonas dla2* mutant by whole-genome sequencing of acetate-requiring mutants found in a collection of photosynthesis mutants. Furthermore, Shtaida et al. (2014) have shown that downregulation of the *Chlamydomonas* E1α subunit (PDC2) significantly reduces the growth rate under photoautotrophic conditions. Since addition of acetate complements the phenotype of *dla2*, the growth deficiency most likely results from insufficient acetyl-CoA production in the mutant. Although usually provided by the cpPDC, acetyl-CoA can alternatively be synthesized by two cpPDC-independent systems, i.e., the acetate synthetase (ACS) and the acetyl-kinase/phosphate acetyltransferase (ACK/PAT) system (Spalding, 2009). Both use acetate as a substrate, thereby bypassing the need for cpPDC's metabolic function under mixotrophic conditions (Spalding, 2009; Yang et al., 2014).

Analysis of the mutant acetylation strains showed that simulated acetylation at K193 and K197 leads to a dramatic reduction in the stability of cpPDC, a concomitant decrease in its metabolic activity, and a decrease in the rate of photoautotrophic growth (Figures 3 and 4; Table 1). In contrast, constitutive deacetylation of K197 enhanced both the stability and activity of cpPDC and moderately increases photoautotrophic growth (Figures 3 and 4; Table 1). However, the differences in photoautotrophic growth between the strains were rather small compared to the significant differences in cpPDC activity *in vitro*. This suggests that additional factors, e.g., CO_2 availability or light intensities, might limit growth under these conditions as well. Nevertheless, addition of acetate reverses the negative effects on growth observed under photoautotrophic conditions, further confirming that cpPDC activity becomes crucial in this context.

The decrease in cpPDC assembly/stability upon simulated acetylation at K193 or K197 shows that these amino acids are crucial for DLA2's interaction with other cpPDC subunits. This is compatible with *in vitro* studies of the E2 subunit of the PDC in *Escherichia coli*, which demonstrated that charge-reverse substitution of the arginine residue corresponding to K193 in DLA2 results in a dramatic reduction in its binding affinity for the respective E1 and E3 proteins (Park et al., 2004). Moreover, mutations of the *Bacillus stearothermophilus* E2 subunit that eliminated the positive charges of the arginine residues corresponding to K193 and K197 in DLA2 showed that mutation of the former led to a massive reduction in E3 binding, while mutation of the latter position resulted in a smaller but still significant decrease (Jung et al., 2002). This, together with our data, shows that acetylation at K197 as well as K193 could enhance cpPDC disassembly, thus facilitating shuttling of DLA2 between its two functions. However, only K197 was found to be differentially acetylated *in vivo*

making it the perfect target for an acetylation-dependent switch between DLA2's two functions (Füßl et al., 2022).

Intriguingly, simulated deacetylation in the *K197R-HA* line increased cpPDC assembly/stability, further substantiating this idea (Figure 4). However, constitutive acetylation of the nearby residue K200 had no significant effect on cpPDC stability or RNA recognition (Figures 3b and 4b; Figure S5; Table 1), perhaps because of its position within the DLA2 structure. A 3D protein structural model generated with the Phyre2 web tool indicates that K193 and K197 reside in an exposed α-helix that would enable interaction with E1 and E3, whereas K200 is located within a loop structure that faces the core of the protein (Figure S13).

Taken together, these findings strongly suggest that reversible lysine acetylation at K197 regulates cpPDC stability/assembly *in vivo*.

Acetylation of DLA2 at K197 forces RNP formation

Several lines of evidence suggest that acetylation of DLA2 at position K197 triggers its release from the destabilized cpPDC and its subsequent association with *psbA* mRNA at membranes. First, analysis of the K197 acetylation strains revealed that the increase in free DLA2 in the *K197Q-HA* line is accompanied by increased levels of membrane-bound DLA2 (Figure 5). In contrast, the increased stability of cpPDC in the *K197R-HA* line results in a decrease in membrane attachment of DLA2 under all growth conditions tested. That increased acetylation at K197 leads to increased membrane attachment of the native DLA2 is supported by the elevated levels of DLA2 found on membranes in the *DLA2-HA* strain under mixotrophic growth conditions in which K197 is progressively acetylated (Füßl et al., 2022; Figure 5). In the presence of acetate, elevated membrane association may be facilitated by the exposure of hydrophobic surfaces of DLA2 upon disassembly of the cpPDC and/or other factors. Secondly, increased membrane association of DLA2 under mixotrophic conditions, and in the constitutively acetylation-mimicking strain *K197Q-HA* even in the absence of acetate, was accompanied by increased RNP formation, while constitutive deacetylation reduced RNP formation as indicated by SEC analyses (Figure 6).

These observations were further supported by FRET microscopy-based imaging of DLA2–*psbA* mRNA interactions at the single-cell level (Figure 7). FRET analysis showed that disassembly of the cpPDC upon acetylation at K197 directly leads to elevated RNP formation around the chloroplast's pyrenoid. The effects were consistent under both mixotrophic and phototrophic growth conditions, suggesting that detectable amounts of the DLA2-containing RNPs are present in the *DLA2-HA* strain even under photoautotrophic conditions, despite its apparent absence in SEC elution profiles (Figure 6, right panel and Figure 7b). Interestingly, the interaction of DLA2 variants with *psbA* mRNA in both K197 acetylation strains was generally higher under mixotrophic than under photoautotrophic conditions (Figure 7). This suggests that there must be an additional determinant that promotes RNP formation in an acetate-dependent manner, which might include unidentified acetylation sites at DLA2, other cpPDC subunits, and/or unknown factors. The acetylome analysis performed by Füßl et al. (2022) did not identify any acetylation site in PDC2 or PDH2, whereas DLD2 was found to be acetylated at K419. Although no evidence for differential modification of K419 was obtained, it is striking that K419 is located within the C-terminal dimerization domain of DLD2. Homodimer formation of E3 subunits has previously been shown to be important for E3 function and E2 binding (Brautigam et al., 2005; Chandrasekhar et al., 2013).

Moreover, experiments performed by Bohne et al. (2013b) suggest that RNP formation also depends on light, which would require an additional light-dependent regulatory element. This might involve phosphorylation(s), since DLA2 has been identified as being phosphorylated under mixotrophic conditions in several independent phosphoproteomic screens (Roustan and Weckwerth, 2018; Wagner et al., 2006; Wang et al., 2014). Furthermore, redox regulation might be involved as well, as DLA2, DLD2, and PDH2 have been shown to be targets of thioredoxin in *Chlamydomonas* (Pérez-Pérez et al., 2017).

The enormous size of the RNP does also not exclude the possibility that additional proteins are involved in RNP formation. Interestingly, SEC analysis of chloroplast proteins from *A. thaliana* revealed that LTA2, the E2 subunit of its cpPDC, forms part of a second HMW complex that is distinct from the cpPDC (Olinares et al., 2010). The fraction characterized by this second HMW complex contained several ribosomal and RNA-binding proteins, e.g., CSP41B, which was shown to interact with numerous mRNAs coding for photosynthetic proteins (Chevalier et al., 2015; Qi et al., 2011). More recently McDermott et al. (2019) co-precipitated the LTA2 protein together with a number of other ribonucleoproteins in a pull-down assay targeting *psbA* mRNA. In summary, the acetylation state of K197 is only one important factor that regulates the moonlighting function of DLA2 and additional factors likely have an impact on cpPDC stability and/or RNP formation in an acetate- and light-dependent manner.

Acetylation at K197 leads to disassembly of the cpPDC and concomitant accumulation of the DLA2/*psbA* mRNA-containing RNP on membranes around the pyrenoid. However, if acetylation of K197 is only required for the destabilization of the cpPDC and the release of DLA2 for RNP formation or if the acetylation of K197 is also a prerequisite for direct membrane association of DLA2 or its interaction with membrane-bound proteins remains to be shown. Interestingly, it has been reported that lysine acetylation can regulate the interaction between proteins and

membranes in both directions. A recent investigation of acetylation and acetylation-mimicking mutations in several peripheral membrane proteins revealed that acetylation of the protein's membrane interaction region strongly reduces its membrane-binding affinity (Okada et al., 2021). The authors accordingly attributed the reduced affinity to the loss of positive charge, which weakens interactions with negatively charged membranes. Contrary, acetylation of certain lysines has also been described to enhance membrane localization of the respective protein (Fischer et al., 2017; Li et al., 2017). This may be due to an increased binding affinity of the protein to more neutral membrane lipids or to a specific binding protein localized at the membrane. In case of DLA2, the latter scenario appears most likely as mimicked acetylation at K197 increased membrane association of the protein. Moreover, the positioning of K197 within the RNA-binding domain makes a simultaneous binding of this region to the membrane unlikely and rather implies the binding to further proteins, which is also supported by the large size of the RNP.

DLA2 regulates D1 synthesis for *de novo* PSII biogenesis

Having shed new light on the mode of *psbA* mRNA-binding by DLA2, we sought to address the question of the function of this RNP. As proposed by Bohne et al. (2013b), DLA2 is responsible for targeting *psbA* mRNA to T-zones around the pyrenoid where *de novo* PSII biogenesis takes place (Schottkowski et al., 2012; Sun et al., 2019; Uniacke and Zerges, 2007, 2009). This hypothesis is supported by the FRET experiments which localize the RNP mainly around the pyrenoid (Figure 7, Figures S9 and S10). Similar to experiments performed on *iDLA2* knockdown lines by Bohne et al. (2013b), the *dla2* knockout line exhibited decreased D1 synthesis in ^{35}S pulse-labeling experiments (Figure 8a). High-light and sulfur starvation experiments suggest that this is due to a reduction in D1 synthesis for *de novo* PSII biogenesis and not for PSII repair (Figure 9 and Figure S12). Interestingly, the major effect observed for *dla2* in sulfur starvation experiments was not a significantly reduced D1 re-accumulation rate, but a delayed response to sulfur repletion under mixotrophic conditions (Figure 9). This suggests that release of DLA2 from cpPDC might be important for facilitation of fast responses to changing environmental conditions. Moreover, it has previously been reported that translation of D1 is induced by the addition of acetate to the medium, i.e., under conditions where the RNP containing DLA2 and *psbA* mRNA is accumulating (Michaels and Herrin, 1990). On the other hand, no alteration in D1 levels was detected under steady-state mixotrophic conditions (Figure 8b), which might be explained by post-translational stabilization effects that counteract the reduced synthesis rate under constant growth conditions. Lastly, it is possible that the observed reduction of D1 synthesis is not due to an actual decrease of translation, but to mislocalization of D1 synthesis, followed by rapid degradation of newly synthesized D1. However, both K197 acetylation mutant strains behaved like the *DLA2-HA* reference strain, indicating that K197 acetylation-dependent formation of the RNP alone is not sufficient to mediate enhanced D1 synthesis (Figure 8a). Additional regulatory steps beyond RNP formation might be required for enhanced D1 synthesis in a light- and acetate-dependent manner. These mechanisms might include other post-translational modifications or additional factors yet to be identified. Furthermore, we cannot exclude the possibility that the small amounts of RNPs present in the *K197R-HA* strain under mixotrophic growth conditions might be sufficient to ensure WT-like levels of D1 synthesis (Figures 7 and 8). Nevertheless, the substantial reduction of D1 synthesis rate in the *dla2* mutant strongly suggests that RNP formation for targeted translation of *psbA* mRNA at T-zones promotes D1 synthesis.

In conclusion, DLA2 is involved in the regulation of D1 synthesis for efficient *de novo* PSII biogenesis, probably at T-zones around the pyrenoid. This makes DLA2 an integrator protein, which coordinates carbon metabolism and gene expression in response to changing environmental conditions, as depicted in Figure 10. Here, reversible lysine acetylation at K197 of DLA2 is a major switch that enables DLA2 to shuttle between its two functions. Future work will dissect the precise impact of growth-dependent alterations of RNP accumulation on D1 synthesis.

EXPERIMENTAL PROCEDURES

Growth of *Chlamydomonas*

Chlamydomonas cultures were grown in Tris–acetate–phosphate medium containing 1% sorbitol (TAPS) under mixotrophic conditions (Harris, 1989). For photoautotrophic growth, cultures were cultivated in HSM medium (Harris, 1989). All liquid cultures were agitated under illumination (30 $\mu E\ m^{-2}\ sec^{-1}$) at 23°C and harvested at a density of around 2×10^6 cells ml^{-1}, unless indicated otherwise.

Antibody generation

To generate antibodies against the PDH2 protein, a fusion protein containing GST was used as the antigen. To construct the expression vector, a DNA fragment coding for amino acids 213–370 of PDH2 was first amplified from cDNA by PCR using the primers PDH2 fw2 BamHI and PDH2 rev EcoRI (Table S1). The resulting fragment was inserted into pGEX4T1 (GE Healthcare, Chicago, IL, USA) via the restriction sites mentioned above. Overexpression was performed in *E. coli* BL21 (DE3) cells at 27°C overnight and the protein was purified with Protino® Glutathione agarose beads (Macherey-Nagel, Düren, Germany) according to the manufacturer's instructions. The resulting protein fraction was used to immunize rabbits to produce polyclonal antiserum (Pineda Antikörper-Service).

Antibodies were raised against DLD2 as described for PDH2. A DNA fragment coding for amino acids 409–585 of the DLD2

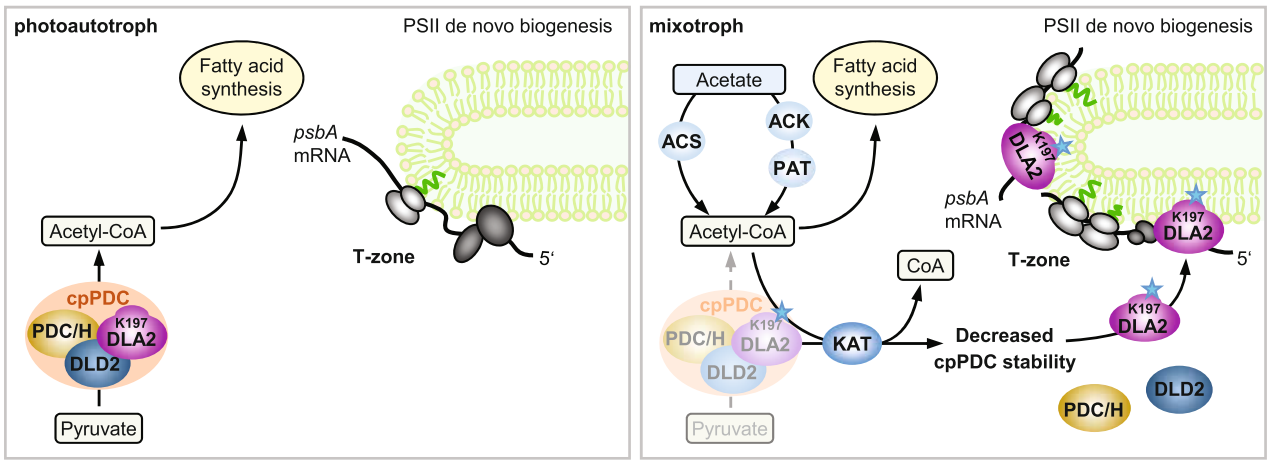

Figure 10. Acetate-dependent regulation of *psbA* gene expression by DLA2 in *Chlamydomonas*. Under photoautotrophic growth conditions, DLA2 is mainly found as subunit of the cpPDC for production of acetyl-CoA, which is needed for fatty acid synthesis (left panel). Under mixotrophic growth conditions, external acetate can be incorporated by the cell and converted into acetyl-CoA by ACS and/or the ACK/PAT system (right panel). Under these conditions, K197 in the E3BD of DLA2 is increasingly acetylated by a protein Lys-*N*-acetyltransferase (KAT), which decreases the stability of the cpPDC and promotes its disassembly. The released DLA2 binds to the *psbA* mRNA and localizes it to T-zones around the pyrenoid, thereby enhancing D1 synthesis for *de novo* biogenesis of PSII. Acetylation at K197 is depicted as a blue star.

protein was amplified using the primers DLD2 fw2 BamHI and DLD2 rev EcoRI (Table S1). The fragment was inserted into pGEX4T1 and overexpressed, and the resulting protein was purified and used to immunize rabbits (Pineda Antikörper-Service).

Chloroplast preparation and SEC

Chloroplast preparation and subsequent SEC of chloroplast extracts with or without RNase treatment were performed basically as described before (Bohne et al., 2013b). Gel filtration samples were loaded through an online filter onto a Sephacryl S500 HR 10 × 300 GL column (GE Healthcare), and elution was performed at 4°C with buffer containing 50 mM KCl, 2.5 mM EDTA, 5 mM ε-aminocaproic acid, 0.1% Triton X-100, and 20 mM Tricine-KOH (pH 7.8) at a flow rate of 0.3 ml min^{-1} using an ÄKTApurifier 10 system (GE Healthcare). Fractions (1 ml) were collected, and 1/10 of each fraction was loaded onto an SDS gel, fractionated electrophoretically, and subjected to immunoblot analysis. To estimate the molecular weights of HMW protein complexes, elution volumes of dextrans with defined molecular weight, specified for the column by the manufacturer, were applied. Proteins from SEC fractions of lysates of the HA-tagged DLA2 lines (Figure 6) were enriched by precipitation by the addition of 20% trichloroacetic acid and incubated for 1 h on ice. The precipitated proteins were then pelleted by centrifugation at 20 000 ***g*** for 20 min and 4°C and washed twice with 80% ice-cold acetone. Subsequently, the protein pellet was dried at 95°C, resuspended in 1× ROTI®Load 1 (Carl Roth GmbH, Karlsruhe, Germany, cat. no. K929.1), and fractionated by SDS-PAGE.

Preparation of *Chlamydomonas* protein extracts

For preparation of total cell lysates, cells were resuspended in lysis buffer (120 mM KCl, 20 mM Tricine pH 7.8, 0.4 mM EDTA) supplemented with 0.5% Triton X-100 and disrupted by sonication (3 × 5 sec) before being subjected to SDS-PAGE. For preparation of membranes, cells were resuspended in lysis buffer without Triton X-100, and cells were homogenized using glass beads and a BeadBug Homogenizer (Biozym Scientific, Hessisch Oldendorf, Germany). Subsequently, the cell lysate was centrifuged at 3000 ***g*** for 5 min to pellet intact cells, the supernatant was transferred to a new tube, and membranes were pelleted by centrifugation at 20 000 ***g*** for 20 min. Membranes were washed twice with lysis buffer and solubilized by resuspension in lysis buffer supplemented with 0.5% Triton X-100. After incubation for 10 min, insoluble particles were removed by centrifugation at 20 000 ***g*** for 10 min and the supernatant was subjected to SDS-PAGE.

Immunoblot analysis

Anti-PDC2 and anti-HSP70B antibodies were kindly provided by Prof. Dr. Peter Nixon (Imperial College London) and Prof. Dr. Michael Schroda (TU Kaiserslautern), respectively. Antibodies against PDH2 and DLD2 were generated for this study (see section on antibody generation). The anti-D2 antibody and the anti-DLA2 antibody have been described previously (Bohne et al., 2013b; Klinkert et al., 2006). Antibodies against D1 (AS11 1786), RbcL (AS03 037), PsaA (AS06 172), and AtpB (AS03 030) were purchased from Agrisera. Secondary horseradish peroxidase (HRP)-conjugated anti-rabbit (A9169) and anti-chicken (A9046) antibodies were purchased from Sigma.

Quantification of the immunoblot signals was performed using ImageQuant software (GE Healthcare).

Generation of plasmid constructs for recombinant protein expression

For the expression of recombinant DLD2 for use in the UV crosslinking experiment, a fragment coding for amino acids 241–585 was amplified using the primers DLD2 fw BamHI and DLD2 rev EcoRI and cloned into the pGEX-4 T-1 plasmid using *Bam*HI and *Eco*RI restriction sites, resulting in the construct pGEX: DLD2 241–585.

All constructs used for the MST experiments were generated by the same procedure. A fragment coding for the respective amino acid sequence was amplified with appropriate primers, using a version of the *DLA2* cDNA adapted to *E. coli* codon usage as a template to increase overexpression. The fragment was cloned into the plasmid pET-28b-SUMO (Bepperling et al., 2012) using *Bam*HI and *Sal*I restriction enzymes. For the pSUMO: DLA2 ΔE3B construct expressing the ΔE3B protein, a 5′-terminal fragment was

amplified using the primers DLA2 cDNA fw 2 BamHI and DLA2-E3B rev SalI and cloned into pET-28b-SUMO, and a 3′-terminal part was amplified using the primers DLA2 -E3B fw SalI and DLA2 cDNA rev SalI, which was subsequently ligated to the 5′-terminal part using the *Sal*I restriction site.

To generate constructs for the expression of acetylation-mutant versions of DLA2, the pSUMO:DLA2 construct was used as the template and nucleotide changes leading to a single amino acid substitution were inserted using the QuikChange XL Site-Directed Mutagenesis Kit (Agilent Technologies) according to the manufacturer's instructions.

For primer sequences see Table S1.

Expression and purification of recombinant proteins

The His-tagged recombinant DLA2 used for the UV crosslinking experiment was expressed as previously described by Bohne et al. (2013b) and purified with Protino® Ni-NTA Agarose beads (Macherey-Nagel) as described above.

For overexpression of the recombinant DLD2 protein, the pGEX: DLD2 241–585 construct was transformed into *E. coli* Rosetta cells (Novagen, Madison, WI, USA). Overexpression was performed at 18°C overnight after induction with 0.5 mM isopropyl β-D-1-thiogalactopyranoside (IPTG). GST-tagged proteins were purified with Protino® Glutathione agarose beads (Macherey-Nagel).

Overexpression of all recombinant proteins used for MST experiments was performed by transformation of the respective constructs into *E. coli* BL21(DE3) cells. Liquid cultures (4 L) were grown to an OD_{600} of 0.6 before induction with 1 mM IPTG and overexpression at 12°C overnight. His-SUMO-tagged proteins were purified with Protino® Ni-NTA agarose beads followed by the removal of the His-SUMO tag by proteolytic digestion with SUMO protease at 4°C overnight.

Microscale thermophoresis

MST was used to quantify the binding affinities of Cy5-labeled *psbA* 5′ UTR probes for WT and mutant DLA2 proteins (Moon et al., 2018; Wienken et al., 2010). Synthetic RNAs were purchased from Metabion International AG. To guarantee high comparability between different samples, all recombinant proteins were overexpressed, purified, and measured at the same time. The concentration of purified recombinant proteins was adjusted to 44 μM using MST buffer (50 mM Tris/HCl pH 7.8, 60 mM KCl, 10 mM $MgCl_2$, 0.05% Tween 20). Subsequently the fluorescently labeled RNA probe was diluted to 20 nM in MST buffer and decreasing amounts of the respective proteins were incubated with the RNA. Samples were then loaded into MST NT.115 premium glass capillaries (NanoTemper, München, Germany) and subjected to thermophoresis at 40% LED power and 20% MST power at room temperature in a Monolith NT.115 instrument (NanoTemper) at the Bioanalytic Service Unit of the Biocenter of the Ludwig-Maximilians-Universität, Munich. K_D values were calculated using MO.Affinity Analysis software (NanoTemper).

In vitro synthesis of RNA and UV crosslinking

In vitro synthesis of RNA and UV crosslinking experiments were performed basically as described by Zerges and Rochaix (1998) and Bohne et al. (2013b). The DNA template for *in vitro* transcription of the *psbA* 5′ UTR RNA probe was generated by PCR using the following primers: T7psbA5 and 2054-psbA (Table S1). Binding reactions (20 μl) were performed at room temperature for 10 min and contained 20 mM HEPES/KOH (pH 7.8), 5 mM $MgCl_2$, 60 mM KCl, and 100 ng of protein. Each reaction contained 100 kcpm of ^{32}P-labeled RNA probe. For competition experiments the indicated amounts of competitor protein were added to the reaction. Radiolabeled RNA and DLA2 were mixed prior to the addition of competing proteins.

cpPDC activity assay

The cpPDC activity assay was based on that described by Bohne et al. (2013b) and performed under conditions that favor the activity of the cpPDC over the mitochondrial PDC (high Mg^{2+} concentration, alkaline pH; Camp and Randall, 1985; Reid et al., 1977). Mixotrophically grown *Chlamydomonas* cultures were harvested and resuspended in PDC lysis buffer (100 mM Tricine pH 8.0, 25 mM $MgCl_2$, 5% [v/v] glycerol). Cells were homogenized using a Bead Bug Homogenizer and soluble protein lysates were prepared by centrifugation at 20 000 ***g*** for 20 min at 4°C. Lysate (200 μg) was added to the reaction mix (0.1 mM thiamine pyrophosphate [TPP], 5 mM $MgCl_2$, 2 mM NAD^+, 0.1 mM acetyl-CoA, 3 mM cysteine, and 0.1 M tricine pH 8.0), and the reaction was started by the addition of 1 mM pyruvate. The change in absorbance at 340 nm indicating NADH production was analyzed for 2 min using an Ultrospec™ 2100 spectrophotometer (GE Healthcare).

Co-immunoprecipitation

Chlamydomonas cells were harvested by centrifugation at 1200 ***g*** at 4°C and resuspended in IP lysis buffer (20 mM Tris/HCl pH 7.8, 150 mM NaCl, 1 mM EDTA, 5% glycerol, and cOmplete™ protease inhibitor cocktail [Roche, Basel, Switzerland]). Cells were lysed using glass beads and a Bead Bug Homogenizer and centrifuged for 20 min at 20 000 ***g*** and 4°C. Then 1.8 mg of the soluble cell extract was incubated with 50 μl of Pierce™ Anti-HA Magnetic Beads (Thermo Fisher Scientific™, Waltham, MA, USA, cat. no. 88836) for 2 h at 4°C on an overhead shaker. Beads were then washed three times with IP lysis buffer, and proteins were eluted with 50 μl 1× non-reducing Roti®-Load 2 (Carl Roth GmbH, cat. no. K930.1) at 45°C for 30 min. Beads were removed and eluates were supplemented with 20 mM DTT and fractionated by SDS-PAGE.

FRET microscopy

FRET was used to visualize DLA2–*psbA* mRNA interactions in various DLA2 mutant lines. Whole *Chlamydomonas* cells were deposited on a borosilicate glass slide (DWK Life Sciences GmbH, Wertheim, Germany). To prevent dehydration, all steps were carried out in a humid box. First, FISH staining was performed, which was adapted from Uniacke et al. (2011). After adherence of the cells to the microscope slide, they were permeabilized in 1× PBS supplemented with 0.5% Tween 20 for 10 min, followed by washing with 1× PBS. For fixation, cells were incubated with 3.7% formaldehyde in 1× PBS for 10 min, followed by two washing steps to remove residual formaldehyde. Subsequently cells were incubated with hybridization solution (1.6× saline sodium citrate [SSC] buffer, 25 μg salmon sperm, 50% formamide, 10 ng each of the four oligonucleotides) overnight at 37°C. Four DNA oligonucleotides each (Table S1) for the hybridization with *psbA* and *psaA* mRNAs described previously by Uniacke and Zerges (2007) were purchased from Sigma-Aldrich and modified by attaching an ATTO 488 fluorescent label to their 5′ ends. On the next day, samples were washed five times: first with 50% formamide in 1× SSC for 30 min at 37°C, then with 1× SSC for 20 min at room temperature, followed by 0.5× SSC for 10 min and two final washes with 1× PBS for 10 min each.

For IF staining, samples were first incubated in blocking solution (5% BSA in 1× PBS) for 1 h, followed by incubation with a

monoclonal antibody against the HA-tag, coupled to a DyLight 550 fluorophore (Thermo Fisher Scientific™, cat. no. 26183D550). Subsequently samples were washed three times with 1× PBS for 10 min. Samples were dried for several hours and incubated overnight with a drop of Calbiochem FluorSave™ Reagent (Merck Millipore) and a high-precision coverslip (Paul Marienfeld GmbH & Co. KG). On the next day, samples were sealed with nail polish and examined on an IX71 inverted microscope (Olympus Deutschland GmbH, Hamburg, Germany) combined with a Delta Vision Elite Filter Set (General Electric Company, Boston, MA, USA) and a CoolSNAP HQ2 camera (Photometrik GmbH, Eppertshausen, Germany). The chromophore label on the *psbA* mRNA was excited at 475/28 nm and emission was measured at 525/48 nm. For detection of the IF of DLA2, the chromophore label was excited at 542/27 nm and emission was measured at 597/45 nm. Consequently, for detection of the FRET signal, the FISH chromophore was excited at 475/28 nm and emission of the IF chromophore was detected at 597/45 nm.

3D reconstruction

A fluorescence micrograph was assembled as a stack of optical sections through the sample and split up into its different wavelength channels. The resulting files were processed and merged by UCSF Chimera (http://www.rbvi.ucsf.edu/chimera) to generate a fully interpolated 3D model of the cell.

Pulse labeling of proteins

Pulse labeling of proteins with ^{35}S was adapted from Bohne et al. (2013a). *Chlamydomonas* liquid cultures were grown to a density of 2×10^6 cells ml^{-1} in TAPS under a fluence of 30 $\mu E\ m^{-2}\ sec^{-1}$ at 23°C. Pulse labeling was performed using 100 mCi $H_2{}^{35}SO_4$ and incubation for 15 min under the same lighting conditions. After centrifugation, the sedimented cells were frozen in liquid nitrogen and resuspended in 100 µl of 1× ROTI®Load 1 sample buffer. After a short burst of sonication (5 sec, room temperature) and incubation for 30 min at room temperature, 10 µl of each sample was loaded onto a 12% SDS-PAGE gel. After electrophoresis, proteins were blotted onto a nitrocellulose membrane (AppliChem GmbH, Darmstadt, Germany, cat. no. A5242) and radioactive signals were detected using phosphorimaging.

Photoinhibition and sulfur starvation

Photoinhibition experiments were performed with liquid cultures (cell density 2×10^6 cells ml^{-1}). Cultures were either supplemented or not with 500 µg ml^{-1} lincomycin and 100 µg ml^{-1} chloramphenicol before exposure to high light (800 $\mu E\ m^{-2}\ sec^{-1}$) for 1.5 h.

Sulfur starvation experiments were performed as described by Muranaka et al. (2015). Cells were harvested at 1000 ***g*** for 10 min, washed twice, resuspended in TAPS-sulfur, and grown for 48 h to induce degradation of PSII. Cells were then shifted back to sulfur-replete conditions and *de novo* synthesis of PSII was monitored for 24 h.

Generation of a *dla2* mutant using the CRISPR/Cas9 system

Mutagenesis was performed on the cell-wall-deficient *Chlamydomonas* strain *CC-3403* (RU-387 *nit1 arg7 cw15* mt-) according to a previously described protocol (Greiner et al., 2017). Transformation was conducted by electroporation, and included a preassembled SpCas9/gRNA complex with a gRNA sequence (UGUUCUGGUGGUCCCCAACG) targeting the Cas9 endonuclease to a restriction site within the first exon of the *DLA2* gene. In addition, an *Arg7* gene cassette was used for selection. After selection on TAP plates without arginine, mutant candidates were picked and screened by colony PCR using the primers DLA2 sl fw and DLA2 sl rev (Table S1). Subsequently, single-cell isolation was conducted for candidate lines that did not show a WT-like PCR fragment pattern, followed by sequencing of the genomic *DLA2* region to confirm the insertion of external DNA. To confirm the absence of the DLA2 protein, immunoblotting with total cell lysates was performed using an anti-DLA2 antibody.

Generation of DLA2 mutant strains

The pBC1:DLA2-HA construct for complementation of the *dla2* knockout mutant was obtained by amplifying a fragment encompassing the entire *DLA2* cDNA using the primers DLA2 fw NdeI and DLA2-3xHA rev EcoRI, thereby adding a triple HA-tag sequence to the 3′ end of the cDNA. The complete *DLA2* cDNA clone (MXL069g06) was purchased from the Kazusa DNA Research Institute, Japan (Asamizu et al., 2004). The resulting fragment was cloned into the pBC1-CrGFP vector (= pJR38, Neupert et al., 2009) using *Nde*I and *Eco*RI restriction sites. A fragment comprising the *DLA2* genomic DNA from the 5′ UTR to the third exon was amplified using the primers DLA2 5′ UTR fw BamHI and DLA2 Exon 3 rev SfiI, and genomic DNA isolated from the *CC-3403* strain was used as the template. Subsequently, the fragment was cloned into the pBC1:DLA2 cDNA-HA plasmid using the restriction sites *Bam*HI and *Sfi*I, replacing the *PsaD* promoter and parts of the *DLA2* cDNA with the 5′ UTR and genomic DNA of the *DLA2* gene. The resulting pBC1:DLA2-HA construct was used as the template for the generation of the acetylation simulation constructs (pBC1:DLA2 K197R-HA, pBC1:DLA2 K197Q-HA, pBC1:DLA2 K193Q-HA, and pBC1:DLA2 K200Q-HA) using the QuikChange XL Site-Directed Mutagenesis Kit according to the manufacturer's instructions. All primer sequences used for the generation of the constructs are listed in Table S1. Obtained constructs were used for complementation of the *dla2* knockout mutant to generate strain *DLA2-HA* and the DLA2 acetylation mutant strains *K197R-HA*, *K197Q-HA*, *K193Q-HA*, and *K200Q-HA*.

For transformation of the *dla2* knockout mutant with the various pBC1:DLA2 constructs, a liquid culture of 100 ml was grown in TAPS to a cell density of approximately 1×10^6 cells ml^{-1}. Cells were harvested and resuspended in MAX Efficiency Transformation Reagent for Algae (Thermo Fisher Scientific) supplemented with 40 µM sucrose to a cell density of 1×10^8 cells ml^{-1}. The cell suspension (250 µl) was transferred to an electroporation cuvette (4 mm gap width, Biozym Scientific) and mixed with 50 µg of denatured salmon sperm and 10 µg of the respective plasmid DNA. The cuvette was incubated for 20 min at 16°C followed by electroporation, which was performed using a Gene Pulser II (Bio-Rad Laboratories, Hercules, CA, USA) with standard settings (resistance = high range; capacity = 10 µF). One pulse with a voltage of 0.8 kV and two additional pulses with a voltage of 0.2 kV were applied, followed by incubation at 16°C for 20 min. Subsequently, cells were recovered in 20 ml of TAPS medium supplemented with 100 µg ml^{-1} ampicillin for 24 h. After the recovery cells were centrifuged at 1000 ***g*** for 10 min and resuspended in 500 µl of HSM medium, the cell suspension was transferred to HSM plates supplemented with 200 µg ml^{-1} of ampicillin, which were incubated at 23°C for 14–21 days for selection of restored photoautotrophic growth.

ACCESSION NUMBERS

Sequence data from this article can be found in public databases under the following accession numbers:

E. coli codon-adapted version of the *DLA2* cDNA, MN642093 (GenBank); *PDH2*, Cre03.g194200 (Phytozome v5.5); *DLD2*, Cre01.g016514 (Phytozome v5.5); *DLA2*, Cre03.g158900 (Phytozome v5.5); *Synechocystis* sp. PCC 6803 protein PratA, slr2048 (CyanoBase).

AUTHOR CONTRIBUTIONS

DN, AVB, PH, and JN designed the experiments. DN, LK, JTT, MO, and SK performed the experiments and analyzed the results. DN, AVB, and JN wrote the paper. JE and IF analyzed and provided acetylation sites for cpPDC subunits in *Chlamydomonas*. SK and PH generated the *dla2* knockout mutant by CRISPR/Cas9.

ACKNOWLEDGMENTS

The authors thank P. Nixon and Michael Schroda for kindly providing PDC2 and HSP70B antisera, respectively, as well as Paul Irmer and Metabion International AG for providing codon-adapted DLA2 cDNA sequences and Krishna K. Niyogi for providing cell-walled *dla2* knockout mutants used for initial verification of phenotypes. We gratefully acknowledge financial support from the Deutsche Forschungsgemeinschaft to JN (TRR175-A06). Open Access funding enabled and organized by Projekt DEAL.

CONFLICT OF INTEREST

The authors declare no conflict of interest.

SUPPORTING INFORMATION

Additional Supporting Information may be found in the online version of this article.

Figure S1. Acetylated and predicted RNA-binding residues in the DLA2 protein from *Chlamydomonas*.

Figure S2. Coomassie brilliant blue-stained SDS gels demonstrating the purification of recombinant proteins used for MST analysis shown in Figure 2b,c.

Figure S3. MST traces and RNA-binding curves of the recombinant DLA2 WT protein (a) and the *Synechocystis* protein PratA (Stengel et al., 2012) as a negative control (b).

Figure S4. MST-binding curves resulting from the interactions of mutant versions of DLA2 with native and mutated C-stretch *psbA* probes.

Figure S5. RNA-binding affinities of various acetylation-mutant versions of DLA2.

Figure S6. Knockout of *DLA2* leads to inhibition of photoautotrophic growth in *Chlamydomonas*.

Figure S7. Western blot analysis showing the accumulation of cpPDC subunits in DLA2 mutant strains.

Figure S8. DLA2 accumulation in soluble fractions of various strains grown under photoautotrophic or mixotrophic conditions.

Figure S9. Fluorescence micrographs of various strains grown under mixotrophic conditions corresponding to Figure 7a.

Figure S10. Fluorescence micrographs of various strains grown under photoautotrophic conditions corresponding to Figure 7b.

Figure S11. Fluorescence micrographs of controls.

Figure S12. Loss of DLA2 has no impact on D1 repair or stability.

Figure S13. 3D structural model of DLA2.

Table S1. Oligonucleotides used in this study.

Movie S1. 3D reconstruction of FRET signals in the *DLA2-HA* strain.

REFERENCES

Asamizu, E., Nakamura, Y., Miura, K., Fukuzawa, H., Fujiwara, S., Hirono, M. et al. (2004) Establishment of publicly available cDNA material and information resource of *Chlamydomonas reinhardtti* (Chlorophyta) to facilitate gene function analysis. *Phycologia*, **43**, 722–726. https://doi.org/10.2216/i0031-8884-43-6-722.1

Barańska, S., Glinkowska, M., Herman-Antosiewicz, A., Maciąg-Dorszyńska, M., Nowicki, D., Szalewska-Pałasz, A. et al. (2013) Replicating DNA by cell factories: roles of central carbon metabolism and transcription in the control of DNA replication in microbes, and implications for understanding this process in human cells. *Microbial Cell Factories*, **12**, 55. https://doi.org/10.1186/1475-2859-12-55

Bennoun, P., Spierer-Herz, M., Erickson, J., Girard-Bascou, J., Pierre, Y., Delosme, M. et al. (1986) Characterization of photosystem II mutants of *Chlamydomonas reinhardtii* lacking the *psbA* gene. *Plant Molecular Biology*, **6**, 151–160. https://doi.org/10.1007/bf00021484

Bepperling, A., Alte, F., Kriehuber, T., Braun, N., Weinkauf, S., Groll, M. et al. (2012) Alternative bacterial two-component small heat shock protein systems. *Proceedings of the National Academy of Sciences of the United States of America*, **109**, 20407–20412. https://doi.org/10.1073/pnas.1209565109

Bohne, A.-V. & Nickelsen, J. (2017) Metabolic control of chloroplast gene expression: an emerging theme. *Molecular Plant*, **10**, 1–3. https://doi.org/10.1016/j.molp.2016.08.002

Bohne, A.-V., Schwarz, C. & Nickelsen, J. (2013a) ^{35}S pulse labelling of Chlamydomonas chloroplast proteins. *Bio-Protocol*, **3**, e783 http://www.Bio-Protocolorg/e783

Bohne, A.-V., Schwarz, C., Schottkowski, M., Lidschreiber, M., Piotrowski, M., Zerges, W. et al. (2013b) Reciprocal regulation of protein synthesis and carbon metabolism for thylakoid membrane biogenesis. *PLoS Biology*, **11**, e1001482. https://doi.org/10.1371/journal.pbio.1001482

Brautigam, C.A., Chuang, J.L., Tomchick, D.R., Machius, M. & Chuang, D.T. (2005) Crystal structure of human dihydrolipoamide dehydrogenase: NAD^+/NADH binding and the structural basis of disease-causing mutations. *Journal of Molecular Biology*, **350**, 543–552. https://doi.org/10.1016/j.jmb.2005.05.014

Camp, P.J. & Randall, D.D. (1985) Purification and characterization of the pea chloroplast pyruvate dehydrogenase complex: a source of acetyl-CoA and NADH for fatty acid biosynthesis. *Plant Physiology*, **77**, 571–577. https://doi.org/10.1104/pp.77.3.571

Chandrasekhar, K., Wang, J., Arjunan, P., Sax, M., Park, Y.-H., Nemeria, N.S. et al. (2013) Insight to the interaction of the dihydrolipoamide acetyltransferase (E2) core with the peripheral components in the *Escherichia coli* pyruvate dehydrogenase complex via multifaceted structural approaches. *The Journal of Biological Chemistry*, **288**, 15402–15417. https://doi.org/10.1074/jbc.M113.466789

Chen, J., Guccini, I., Di Mitri, D., Brina, D., Revandkar, A., Sarti, M. et al. (2018) Compartmentalized activities of the pyruvate dehydrogenase complex sustain lipogenesis in prostate cancer. *Nature Genetics*, **50**, 219–228. https://doi.org/10.1038/s41588-017-0026-3

Chevalier, F., Ghulam, M.M., Rondet, D., Pfannschmidt, T., Merendino, L. & Lerbs-Mache, S. (2015) Characterization of the *psbH* precursor RNAs reveals a precise endoribonuclease cleavage site in the *psbT/psbH* intergenic region that is dependent on *psbN* gene expression. *Plant Molecular Biology*, **88**, 357–367. https://doi.org/10.1007/s11103-015-0325-y

Cohen, I., Sapir, Y. & Shapira, M. (2006) A conserved mechanism controls translation of Rubisco large subunit in different photosynthetic organisms. *Plant Physiology*, **141**, 1089–1097. https://doi.org/10.1104/pp.106.079046

Fischer, A., Mühlhäuser, W.W.D., Warscheid, B. & Radziwill, G. (2017) Membrane localization of acetylated CNK1 mediates a positive feedback on RAF/ERK signaling. *Science Advances*, **3**, e1700475. https://doi.org/10.1126/sciadv.1700475

Füßl, M., König, A.-C., Eirich, J., Hartl, M., Kleinknecht, L., Bohne, A.-V. et al. (2022) Dynamic light- and acetate-dependent regulation of the proteome and lysine acetylome of *Chlamydomonas*. *The Plant Journal*, **109**, 261–277. https://doi.org/10.1111/tpj.15555

Greiner, A., Kelterborn, S., Evers, H., Kreimer, G., Sizova, I. & Hegemann, P. (2017) Targeting of photoreceptor genes in *Chlamydomonas reinhardtii* via zinc-finger nucleases and CRISPR/Cas9. *Plant Cell*, **29**, 2498–2518. https://doi.org/10.1105/tpc.17.00659

Harris, E.H. (1989) *The Chlamydomonas Sourcebook: a comprehensive guide to biology and laboratory use*. San Diego: Academic Press.

He, S., Chou, H.-T., Matthies, D., Wunder, T., Meyer, M.T., Atkinson, N. et al. (2020) The structural basis of Rubisco phase separation in the pyrenoid. *Nature Plants*, **6**, 1480–1490. https://doi.org/10.1038/s41477-020-00811-y

Huranová, M., Jablonski, J.A., Benda, A., Hof, M., Staněk, D. & Caputi, M. (2009) In vivo detection of RNA-binding protein interactions with cognate RNA sequences by fluorescence resonance energy transfer. *RNA*, **15**, 2063–2071. https://doi.org/10.1261/rna.1678209

Jeffery, C.J. (2003) Moonlighting proteins: old proteins learning new tricks. *Trends in Genetics*, **19**, 415–417. https://doi.org/10.1016/S0168-9525(03)00167-7

Jung, H.-I., Cooper, A. & Perham, R.N. (2002) Identification of key amino acid residues in the assembly of enzymes into the pyruvate dehydrogenase complex of *Bacillus stearothermophilus*: a kinetic and thermodynamic analysis. *Biochemistry*, **41**, 10446–10453. https://doi.org/10.1021/bi020147y

Kim, J.-W. & Dang, C.V. (2005) Multifaceted roles of glycolytic enzymes. *Trends in Biochemical Sciences*, **30**, 142–150. https://doi.org/10.1016/j.tibs.2005.01.005

Kleine, T., Nägele, T., Neuhaus, H.E., Schmitz-Linneweber, C., Fernie, A.R., Geigenberger, P. et al. (2021) Acclimation in plants - the Green Hub consortium. *The Plant Journal*, **106**, 23–40. https://doi.org/10.1111/tpj.15144

Klinkert, B., Elles, I. & Nickelsen, J. (2006) Translation of chloroplast *psbD* mRNA in Chlamydomonas is controlled by a secondary RNA structure blocking the AUG start codon. *Nucleic Acids Research*, **34**, 386–394. https://doi.org/10.1093/nar/gkj433

König, A.-C., Hartl, M., Boersema, P.J., Mann, M. & Finkemeier, I. (2014) The mitochondrial lysine acetylome of Arabidopsis. *Mitochondrion*, **19**, 252–260. https://doi.org/10.1016/j.mito.2014.03.004

Li, Y.-T., Yi, C., Chen, C.-C., Lan, H., Pan, M., Zhang, S.-J. et al. (2017) A semisynthetic Atg3 reveals that acetylation promotes Atg3 membrane binding and Atg8 lipidation. *Nature Communications*, **8**, 14846. https://doi.org/10.1038/ncomms14846

Lorenz, M. (2009) Visualizing protein–RNA interactions inside cells by fluorescence resonance energy transfer. *RNA*, **15**, 97–103. https://doi.org/10.1261/rna.1307809

Malnoë, A., Wang, F., Girard-Bascou, J., Wollman, F.-A. & de Vitry, C. (2014) Thylakoid FtsH protease contributes to photosystem II and cytochrome *b6f* remodeling in *Chlamydomonas reinhardtii* under stress conditions. *Plant Cell*, **26**, 373–390. https://doi.org/10.1105/tpc.113.120113

McDermott, J.J., Watkins, K.P., Williams-Carrier, R. & Barkan, A. (2019) Ribonucleoprotein capture by in vivo expression of a designer Pentatricopeptide Repeat Protein in *Arabidopsis*. *Plant Cell*, **31**, 1723–1733. https://doi.org/10.1105/tpc.19.00177

Michaels, A. & Herrin, D.L. (1990) Translational regulation of chloroplast gene expression during the light-dark cell cycle of Chlamydomonas: evidence for control by ATP/energy supply. *Biochemical and Biophysical Research Communications*, **170**, 1082–1088. https://doi.org/10.1016/0006-291x(90)90503-f

Mo, R., Yang, M., Chen, Z., Cheng, Z., Yi, X., Li, C. et al. (2015) Acetylome analysis reveals the involvement of lysine acetylation in photosynthesis and carbon metabolism in the model cyanobacterium *Synechocystis sp.* PCC 6803. *Journal of Proteome Research*, **14**, 1275–1286. https://doi.org/10.1021/pr501275a

Moon, M.H., Hilimire, T.A., Sanders, A.M. & Schneekloth, J.S. (2018) Measuring RNA–ligand interactions with microscale thermophoresis. *Biochemistry*, **57**, 4638–4643. https://doi.org/10.1021/acs.biochem.7b01141

Mooney, B.P., Miernyk, J.A. & Randall, D.D. (1999) Cloning and characterization of the dihydrolipoamide S-acetyltransferase subunit of the plastid pyruvate dehydrogenase complex (E2) from Arabidopsis. *Plant Physiology*, **120**, 443–452. https://doi.org/10.1104/pp.120.2.443

Muranaka, L.S., Rütgers, M., Bujaldon, S., Heublein, A., Geimer, S., Wollman, F.-A. et al. (2015) Tef30 interacts with photosystem II monomers and is involved in the repair of photodamaged photosystem II in *Chlamydomonas reinhardtii*. *Plant Physiology*, **170**, 821–840. https://doi.org/10.1104/pp.15.01458

Neupert, J., Karcher, D. & Bock, R. (2009) Generation of *Chlamydomonas* strains that efficiently express nuclear transgenes. *The Plant Journal*, **57**, 1140–1150. https://doi.org/10.1111/j.1365-313X.2008.03746.x

Okada, A.K., Teranishi, K., Ambroso, M.R., Isas, J.M., Vazquez-Sarandeses, E., Lee, J.-Y. et al. (2021) Lysine acetylation regulates the interaction between proteins and membranes. *Nature Communications*, **12**, 6466. https://doi.org/10.1038/s41467-021-26657-2

Olinares, P.D.B., Ponnala, L. & van Wijk, K.J. (2010) Megadalton complexes in the chloroplast stroma of *Arabidopsis thaliana* characterized by size exclusion chromatography, mass spectrometry and hierarchical clustering. *Molecular & Cellular Proteomics*, **9**, 1594–1615. https://doi.org/10.1074/mcp.M000038-MCP201

Ossenbühl, F., Hartmann, K. & Nickelsen, J. (2002) A chloroplast RNA binding protein from stromal thylakoid membranes specifically binds to the 5′ untranslated region of the *psbA* mRNA. *European Journal of Biochemistry*, **269**, 3912–3919. https://doi.org/10.1046/j.1432-1033.2002.03057.x

Park, Y.-H., Wei, W., Zhou, L., Nemeria, N. & Jordan, F. (2004) Amino-terminal residues 1–45 of the *Escherichia coli* pyruvate dehydrogenase complex E1 subunit interact with the E2 subunit and are required for activity of the complex but not for reductive acetylation of the E2 subunit. *Biochemistry*, **43**, 14037–14046. https://doi.org/10.1021/bi049027b

Patel, M.S., Nemeria, N.S., Furey, W. & Jordan, F. (2014) The pyruvate dehydrogenase complexes, structure-based function and regulation. *The Journal of Biological Chemistry*, **289**, 16615–16623. https://doi.org/10.1074/jbc.R114.563148

Pérez-Pérez, M.E., Mauriès, A., Maes, A., Tourasse, N.J., Hamon, M., Lemaire, S.D. et al. (2017) The deep thioredoxome in *Chlamydomonas reinhardtii*: New insights into redox regulation. *Molecular Plant*, **10**, 1107–1125. https://doi.org/10.1016/j.molp.2017.07.009

Qi, Y., Armbruster, U., Schmitz-Linneweber, C., Delannoy, E., de Longevialle, A.F., Rühle, T. et al. (2011) Arabidopsis CSP41 proteins form multimeric complexes that bind and stabilize distinct plastid transcripts. *Journal of Experimental Botany*, **63**, 1251–1270. https://doi.org/10.1093/jxb/err347

Reid, E.E., Thompson, P., Lyttle, C.R. & Dennis, D.T. (1977) Pyruvate dehydrogenase complex from higher plant mitochondria and proplastids. *Plant Physiology*, **59**, 842–848. https://doi.org/10.1104/pp.59.5.842

Ren, Q. & Gorovsky, M.A. (2001) Histone H2A.Z acetylation modulates an essential charge patch. *Molecular Cell*, **7**, 1329–1335. https://doi.org/10.1016/S1097-2765(01)00269-6

Richard, A.J., Hang, H. & Stephens, J.M. (2017) Pyruvate dehydrogenase complex (PDC) subunits moonlight as interaction partners of phosphorylated STAT5 in adipocytes and adipose tissue. *The Journal of Biological Chemistry*, **292**, 19733–19742. https://doi.org/10.1074/jbc.M117.811794

Roustan, V. & Weckwerth, W. (2018) Quantitative phosphoproteomic and system-level analysis of tor inhibition unravel distinct organellar acclimation in *Chlamydomonas reinhardtii*. *Frontiers in Plant Science*, **9**, 1590. https://doi.org/10.3389/fpls.2018.01590

Schmid, L.-M., Ohler, L., Möhlmann, T., Brachmann, A., Muiño, J.M., Leister, D. et al. (2019) PUMPKIN, the sole plastid ump kinase, associates with group II introns and alters their metabolism. *Plant Physiology*, **179**, 248–264. https://doi.org/10.1104/pp.18.00687

Schottkowski, M., Peters, M., Zhan, Y., Rifai, O., Zhang, Y. & Zerges, W. (2012) Biogenic membranes of the chloroplast in *Chlamydomonas reinhardtii*. *Proceedings of the National Academy of Sciences of the United States of America*, **109**, 19286–19291. doi:10.1073/pnas.1209860109. https://doi.org/10.1073/pnas.1209860109

Sekine, K., Hase, T. & Sato, N. (2002) Reversible DNA compaction by sulfite reductase regulates transcriptional activity of chloroplast nucleoids. *The Journal of Biological Chemistry*, **277**, 24399–24404. https://doi.org/10.1074/jbc.M201714200

Shtaida, N., Khozin-Goldberg, I., Solovchenko, A., Chekanov, K., Didi-Cohen, S., Leu, S. et al. (2014) Downregulation of a putative plastid PDC E1α subunit impairs photosynthetic activity and triacylglycerol accumulation in nitrogen-starved photoautotrophic *Chlamydomonas reinhardtii*. *Journal of Experimental Botany*, **65**, 6563–6576. https://doi.org/10.1093/jxb/eru374

Smith-Hammond, C.L., Swatek, K.N., Johnston, M.L., Thelen, J.J. & Miernyk, J.A. (2014) Initial description of the developing soybean seed

protein Lys-Nε-acetylome. *Journal of Proteomics*, **96**, 56–66. https://doi.org/10.1016/j.jprot.2013.10.038

Spalding, M.H. (2009) The CO_2-concentrating mechanism and carbon assimilation. In: Stern, D.B. (Ed.) *The Chlamydomonas sourcebook: organellar and metabolic processes*, Vol. **2**. Amsterdam: Elsevier Inc., pp. 257–301.

Stengel, A., Gügel, I.L., Hilger, D., Rengstl, B., Jung, H. & Nickelsen, J. (2012) Initial steps of photosystem II de novo assembly and preloading with manganese take place in biogenesis centers in Synechocystis. *Plant Cell*, **24**, 660–675. https://doi.org/10.1105/tpc.111.093914

Sun, Y., Valente-Paterno, M., Bakhtiari, S., Law, C., Zhan, Y. & Zerges, W. (2019) Photosystem biogenesis is localized to the translation zone in the chloroplast of *Chlamydomonas*. *Plant Cell*, **31**, 3057–3072. https://doi.org/10.1105/tpc.19.00263

Treede, H.-J. & Heise, K.-P. (1986) Purification of the chloroplast pyruvate dehydrogenase complex from spinach and maize mesophyll. *Zeitschrift für Naturforschung. Section C*, **41**, 1011–1017. https://doi.org/10.1515/znc-1986-11-1210

Uniacke, J., Colón-Ramos, D. & Zerges, W. (2011) FISH and immunofluorescence staining in Chlamydomonas. In: Gerst, J.E. (Ed.) *RNA Detection and Visualization*, Vol. **714**. Totowa: Humana Press, pp. 15–29. https://doi.org/10.1007/978-1-61779-005-8_2

Uniacke, J. & Zerges, W. (2007) Photosystem II assembly and repair are differentially localized in Chlamydomonas. *Plant Cell*, **19**, 3640–3654. https://doi.org/10.1105/tpc.107.054882

Uniacke, J. & Zerges, W. (2009) Chloroplast protein targeting involves localized translation in Chlamydomonas. *Proceedings of the National Academy of Sciences of the United States of America*, **106**, 1430–1444. https://doi.org/10.1073/pnas.0811268106

Wagner, V., Gessner, G., Heiland, I., Kaminski, M., Hawat, S., Scheffler, K. et al. (2006) Analysis of the phosphoproteome of *Chlamydomonas reinhardtii* provides new insights into various cellular pathways. *Eukaryotic Cell*, **5**, 457–468. https://doi.org/10.1128/ec.5.3.457-468.2006

Wakao, S., Shih, P.M., Guan, K., Schackwitz, W., Ye, J., Patel, D. et al. (2021) Discovery of photosynthesis genes through whole-genome sequencing of acetate-requiring mutants of *Chlamydomonas reinhardtii*. *PLoS Genetics*, **17**, e1009725. https://doi.org/10.1371/journal.pgen.1009725

Wang, H., Gau, B., Slade, W.O., Juergens, M., Li, P. & Hicks, L.M. (2014) The global phosphoproteome of *Chlamydomonas reinhardtii* reveals complex organellar phosphorylation in the flagella and thylakoid membrane. *Molecular & Cellular Proteomics*, **13**, 2337–2353. https://doi.org/10.1074/mcp.M114.038281

Wang, Y., Stessman, D.J. & Spalding, M.H. (2015) The CO_2 concentrating mechanism and photosynthetic carbon assimilation in limiting CO_2: how *Chlamydomonas* works against the gradient. *The Plant Journal*, **82**, 429–448. https://doi.org/10.1111/tpj.12829

Wellen, K.E. & Thompson, C.B. (2012) A two-way street: reciprocal regulation of metabolism and signalling. *Nature Reviews. Molecular Cell Biology*, **13**, 270–276. https://doi.org/10.1038/nrm3305

Wienken, C.J., Baaske, P., Rothbauer, U., Braun, D. & Duhr, S. (2010) Protein-binding assays in biological liquids using microscale thermophoresis. *Nature Communications*, **1**, 100. https://doi.org/10.1038/ncomms1093

Yan, Z., Shen, Z., Gao, Z.-F., Chao, Q., Qian, C.-R., Zheng, H. et al. (2020) A comprehensive analysis of the lysine acetylome reveals diverse functions of acetylated proteins during de-etiolation in Zea mays. *Journal of Plant Physiology*, **248**, 153158. https://doi.org/10.1016/j.jplph.2020.153158

Yang, W., Catalanotti, C., D'Adamo, S., Wittkopp, T.M., Ingram-Smith, C.J., Mackinder, L. et al. (2014) Alternative acetate production pathways in *Chlamydomonas reinhardtii* during dark anoxia and the dominant role of chloroplasts in fermentative acetate production. *Plant Cell*, **26**, 4499–4518. https://doi.org/10.1105/tpc.114.129965

Zerges, W. & Rochaix, J.-D. (1998) Low density membranes are associated with RNA-binding proteins and thylakoids in the chloroplast of *Chlamydomonas reinhardtii*. *The Journal of Cell Biology*, **140**, 101–110. https://doi.org/10.1083/jcb.140.1.101

Zhan, Y., Dhaliwal, J.S., Adjibade, P., Uniacke, J., Mazroui, R. & Zerges, W. (2015) Localized control of oxidized RNA. *Journal of Cell Science*, **128**, 4210–4219. https://doi.org/10.1242/jcs.175232

Zhou, Z.H., McCarthy, D.B., O'Connor, C.M., Reed, L.J. & Stoops, J.K. (2001) The remarkable structural and functional organization of the eukaryotic pyruvate dehydrogenase complexes. *Proceedings of the National Academy of Sciences of the United States of America*, **98**, 14802–14807. https://doi.org/10.1073/pnas.011597698